The Canadian Mineralogist
Vol. 48, pp. 887-923 (2010)
DOI: 10.3749/canmin.48.4.887

PETROLOGY, GEOCHEMISTRY, AND STRUCTURE OF THE CHUGWATER ANORTHOSITE, LARAMIE ANORTHOSITE COMPLEX, SOUTHEASTERN WYOMING

DONALD H. LINDSLEY§

Department of Geosciences and Mineral Physics Institute, Stony Brook University, Stony Brook, New York 11794-2100, USA

B. RONALD FROST AND CAROL D. FROST

Department of Geology and Geophysics, University of Wyoming, Laramie, Wyoming 82071, USA

JAMES S. SCOATES

Department of Earth and Ocean Sciences, University of British Columbia, Vancouver, British Columbia V6T 1Z4, Canada

ABSTRACT

The Chugwater Anorthosite is one of several 1.43 Ga intrusions that make up the Laramie Anorthosite Complex in the Laramie Mountains, Wyoming, USA. The southwestern portion of the Chugwater Anorthosite has a mappable magmatic stratigraphy totaling at least 8000 meters, and probably 10,000 m or more. It consists of three major units, each of which comprises a lower, dominantly anorthosite portion (>90 vol.% plagioclase) and an upper, dominantly gabbroic anorthosite section (80–90 vol.% plagioclase). Each anorthosite portion contains layers of gabbroic anorthosite and *vice versa*, on a variety of scales ranging down to centimeters. Plagioclase is dominantly $An_{50–55}$, although higher and lower values are also found. This "main series" of the Chugwater Anorthosite mainly lacks modal and normative olivine. Oxygen fugacity ranged from FMQ to FMQ + 0.5. We interpret that the "main series" was produced by at least three major injections of mildly hyperfeldspathic magma containing approximately 40% entrained plagioclase megacrysts (tabular crystals at least 5 cm across). The Ti contents of the megacrysts (0.3–0.4 wt% TiO_2) suggest that these had crystallized at pressures near 10 kbar, consistent with initial formation in a magma chamber at or near the base of the crust. Emplacement pressure is poorly constrained, but appears to have been near 3.5–4 kbar. However, before the main series had completely solidified, it was repeatedly intruded by at least two (and probably more) leucotroctolitic magmas. Contacts of leucotroctolite are sharp against anorthosite, but commonly are diffuse against gabbroic anorthosite, suggesting that sufficient residual melt remained in the latter to permit local mixing with leucotroctolite. We estimate that 80–85% of the Chugwater Anorthosite is main-series, 10–15% is mixed rock, and 5% is leucotroctolite. Prior to final solidification, the entire Chugwater Anorthosite was domed, probably as a result of gravitational instability of the relatively buoyant plagioclase-rich material. The emplacement of the Chugwater Anorthosite as a series of crystal-rich magmas, followed by continued fractionation in a magma chamber at a mid-crustal level and subsequent doming, are characteristics that make the Chugwater Anorthosite intermediate between the Poe Mountain Anorthosite to the north (*in situ* fractionation in a magma chamber) and the classic diapiric emplacement of a crystal-rich mush.

Keywords: anorthosite, gabbroic anorthosite, leucotroctolite, plagioclase, layering, magmatic stratigraphy, magma mixing, filter pressing, Chugwater pluton, Wyoming.

SOMMAIRE

L'anorthosite de Chugwater est un des nombreux massifs intrusifs qui constituent le complexe anorthositique de Laramie, au Wyoming, mis en place il y a 1.43 milliard d'années. La partie du complexe de Chugwater se trouvant au sud-ouest du pluton contient une stratigraphie magmatique cartographiable sur une épaisseur d'environ au moins 8,000 mètres, et probablement même jusqu'à 10,000 m ou plus. Nous définissons trois unités majeures, chacune comprenant une portion inférieure à dominance anorthositique (>90% plagioclase par volume) et une unité supérieure surtout à anorthosite gabbroïque (80–90% plagioclase). Chaque portion anorthositique contient des couches d'anorthosite gabbroïque et *vice versa*, dont l'échelle s'étend jusqu'au centimètre. Le plagioclase se rapproche de $An_{50–55}$, quoique des valeurs plus élevées et plus faibles sont aussi présentes. Cette "série principale" du massif de Chugwater est en général dépourvue d'olivine modale et normative. La fugacité de l'oxygène a varié entre le tampon FMQ et FMQ + 0.5. Nous interprétons cette "série principale" comme résultat de trois venues majeures

§ *E-mail address*: donald.lindsley@stonybrook.edu

de magma légèrement hyperfeldspathique contenant environ 40% de mégacristaux de plagioclase apportés (cristaux tabulaires mesurant au moins 5 cm). Leur teneur en Ti (0.3–0.4% TiO_2, poids) fait penser que ces mégacristaux se sont formés à une pression voisine de 10 kbar, ce qui concorderait avec une formation précoce dans une chambre magmatique située près de la base de la croûte. La pression de la mise en place n'est pas bien contrôlée, mais semble avoir été voisine de 3.5–4 kbar. Toutefois, avant que la série principale ait eu la chance de se solidifier complètement, elle a été recoupée par au moins deux venues de magma leucotroctolitique. Les contacts de l'anorthosite avec la leucotroctolite sont francs, mais diffus avec le gabbro anothositique, ce qui fait penser qu'il existait une fraction suffisante de liquide résiduel pour permettre un mélange local avec la leucotroctolite. Nous croyons que 80–85% de l'anorthosite de Chugwater est faite de cette série principale, 10–15% est une roche mixte, et 5% est une leucotroctolite. Avant que soit terminée la solidification finale, le complexe au complet a été domé, probablement suite à l'instabilité gravitationnelle des roches riches en plagioclase, à densité plutôt faible. L'anorthosite de Chugwater se serait mise en place de sous forme de venues de magmas riches en cristaux, sujettes à un fractionnement continu dans une chambre magmatique au niveau de la croûte moyenne et à une montée en dome. Ces caractéristiques seraient intermédiaires entre le cas de l'anorthosite de Poe Mountain au nord (fractionnement *in situ* dans une chambre magmatique) et la mise en place diapirique classique d'une suspension magmatique riche en cristaux.

(Traduit par la Rédaction)

Mots-clés: anorthosite, anorthosite gabbroïque, leucotroctolite, plagioclase, litage, stratification magmatique, mélange de magmas, effet de filtre presse, pluton de Chugwater, Wyoming.

Introduction

Proterozoic massif anorthosites have long intrigued petrologists, both for the enigmas posed by their plagioclase-rich nature and for the distinctive suites of rocks that almost invariably accompany them. Clearly they formed by igneous processes, but, as pointed out by Bowen (1917), they cannot have formed from a magma of their own bulk composition. Some mechanism must concentrate huge volumes of plagioclase to make anorthosites possible. During the past 40 years, a remarkable consensus has developed on a two-stage model for their origin (Morse 1968, Emslie 1985, Longhi & Ashwal 1985, Emslie *et al.* 1994): magma, probably basaltic, ponds and differentiates at or near the base of the crust, crystallizing olivine and pyroxene. These ferromagnesian phases sink, leaving the residual magma enriched in plagioclase components and in iron relative to magnesium. Plagioclase eventually crystallizes and floats to the top of the magma chamber; the buoyant plagioclase with some trapped liquid then ascends diapirically into the crust. Finally, much of the trapped liquid is expelled through a vague process known as "filter-pressing", and the result is anorthosite, an igneous rock containing more than 90% plagioclase.

Although the Morse – Emslie – Longhi – Ashwal model described above successfully explains many massif anorthosites, there are exceptions. Scoates (1994, 2000, Scoates *et al.* 2010) has shown unequivocally that the Poe Mountain Anorthosite of the Laramie Anorthosite complex in southeastern Wyoming crystallized mainly *in situ* within a mid-crustal-level magma chamber. We describe here the Chugwater Anorthosite, which outcrops south of the Poe Mountain Anorthosite, and which also shows magmatic layering and magmatic stratigraphy. However, the Chugwater Anorthosite shows abundant evidence of solid-state deformation and lacks clear evidence, such as scours or blocks that behaved as "drop-stones" on the underlying semi-consolidated cumulates, of having formed in an open magma chamber. As such, it appears to be intermediate between the layered-intrusion nature of the Poe Mountain Anorthosite and the diapiric origin of many other massif anorthosites (*e.g.,* Barnichon *et al.* 1999). As suggested by Wiebe (1992, p. 225), there appears to be a continuum of emplacement modes for Proterozoic anorthosites.

Geological Setting and Previous Work

The Chugwater Anorthosite is one of several plagioclase-rich intrusions in the southern Laramie Mountains that, together with a number of granitic and monzonitic bodies, make up the youngest Precambrian rocks of southeastern Wyoming. These intrusions straddle the Cheyenne Belt, cutting Archean rocks to the north and northwest (Fig. 1) and Proterozoic rocks to the south. Elsewhere, their contacts are mainly covered by Phanerozoic sediments. Darton *et al.* (1910) were the first to report anorthositic rocks in the area, although the presence of the closely associated Fe–Ti oxide ore deposits had been known since the Hayden Survey of 1871. Fowler (1930a, 1930b) made the first detailed study of the anorthosites. Newhouse & Hagner (1957) mapped the area at a scale of one mile to the inch (1:63,360) and identified a northern and a smaller southern anorthositic mass. They suggested that the northern anorthosite forms a doubly-plunging anticline, with an "anticlinal axis" oriented approximately north–south. They reported that most of the major oxide deposits occur on or near this axis. The name Laramie Anorthosite Complex (LAC) was first applied to the entire area by Hodge *et al.* (1973). Whereas Fowler (1930a, 1930b) recognized the magmatic nature of these rocks, some later workers argued that they are metasomatic (Newhouse & Hagner 1957). Klugman

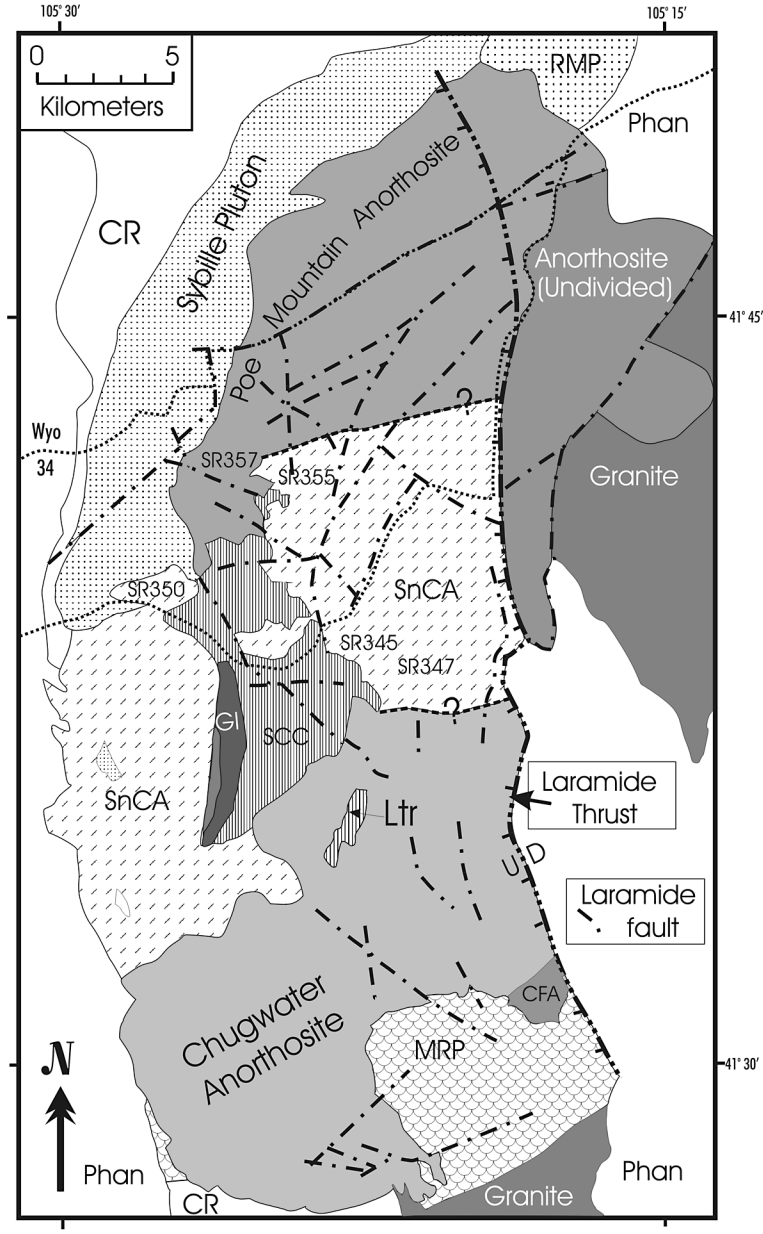

FIG. 1. Simplified geological map of the Laramie Anorthosite Complex, southeastern Wyoming, showing the position of the Chugwater Anorthosite. Abbreviations: CR: Archean (north) and Proterozoic (south) country rock, RMP: Red Mountain Pluton, Phan: Phanerozoic sediments, SnCA: Snow Creek Anorthosite, SCC: Strong Creek complex, GI: Greaser Intrusion, Ltr: leucotroctolite (olivine anorthosite of Newhouse & Hagner 1957), CFA: Coyote Flats Anorthosite, MRP: Maloin Ranch Pluton. Major Laramide faults are indicated. Dotted lines show major roads. Not labeled: Buttes Granite (immediately west of GI) and two small bodies of monzosyenite (in SnCA and west of Chugwater Anorthosite), with similarities to the Sybille Pluton.

(1969) restated the case for magmatic origin, and with the exception of DeVore (1975), who argued that the anorthosites are refractory residues after partial melting of metasediments, subsequent workers have accepted their igneous nature. Subbarayudu (1975) and Subbarayudu *et al*. (1975) conducted the first Rb–Sr isotopic studies of the LAC, whereas Fountain *et al*. (1981) and Goldberg (1984) presented geochemical results for monzonitic and anorthositic rocks in the northern part of the plutonic suite.

We have been studying the LAC since 1981, with most of our earlier efforts concentrating on the granitic and monzonitic rocks of the area (see references in Frost *et al*. 1993). Scoates (1994) conducted a detailed study of northernmost body of anorthosite (the "northern dome" of Frost *et al*. 1993), which he named the Poe Mountain Anorthosite. He showed that the Poe Mountain Anorthosite has a distinctive magmatic stratigraphy and concluded that it had mainly crystallized *in situ* in a mid-crustal-level magma chamber (Scoates & Frost 1996, Scoates 2000, Scoates *et al*. 2010). This is in contrast to the widely accepted notion that massif anorthosites are emplaced as diapiric crystal mushes (*e.g.*, Emslie 1985, Longhi & Ashwal 1985, Ashwal 1993, Barnichon *et al*. 1999). Scoates & Chamberlain (1995, 1997) used U–Pb ages from zircon and baddeleyite to show that the southern anorthosite (the "southern dome" of Frost *et al*. 1993) is distinctly older than the northern anorthosites (1756 Ma compared to 1434–1436 Ma). Accordingly, they named the older body the Horse Creek Anorthosite (see also Frost *et al*. 2000), and suggested that the term Laramie Anorthosite Complex be restricted to the younger rocks to the north (see also Frost *et al*. 2000).

Areal Extent and Relationship to Other Units

The Chugwater Anorthosite is named for its exposure along the banks of Middle and South Chugwater creeks. Approximately 160 km^2 in areal extent, it outcrops in parts of the Baldy Mountain, King Mountain, Goat Mountain, and Ragged Top Mountain 1:24,000 USGS quadrangles. Its southern contact lies mainly on land closed to us, but it appears to intrude a complex series of Proterozoic supracrustal rocks and possibly monzonitic rocks associated with the Horse Creek Anorthosite to the south (Fig. 2). To the southeast, it is cut by the monzonites and granites of the Maloin Ranch Pluton (Kolker & Lindsley 1989). Its foliation is also cut by the small Coyote Flats Anorthosite. The southern portion of its west margin is cut by poorly exposed rocks that are similar to the Maloin Ranch Pluton and the Sybille intrusion, whereas farther north, all igneous rocks are covered by Phanerozoic sediments. To the northwest, the Chugwater Anorthosite is cut by the Snow Creek Anorthosite (the "Snow Creek dome" of Frost *et al*. 1993) and by the Strong Creek Pluton. Both contacts are poorly exposed, but there appears to have been considerable mingling between these units, as indicated by abundant inclusions of Chugwater Anorthosite within the younger units. We suspect but cannot prove that there was also back-intrusion of the younger units into the Chugwater Anorthosite. The northern contact is problematic, as both exposure and sample density are poor; we tentatively place it mainly along Strong Creek. The eastern contacts are mainly Laramide faults along which the Chugwater Anorthosite has been thrust over Phanerozoic sediments. There is permissive evidence from petrography and Pb isotopes that at least part of the "anorthosite undivided" east of the thrusts in Figure 1 may be Chugwater Anorthosite (Frost *et al*. 2010).

Exposures, outcrop, and sampling

Outcrops of the Chugwater Anorthosite are not all one could wish for. Although exposure is commonly adequate for reconnaissance mapping, rarely can one trace units in detail or find clear contacts. Weathering has been sufficiently intense that fresh rock outcrops mainly only in stream beds, and there it may be impossible to sample adequately except by drilling. Most of the samples reported in this paper, and nearly all those for which whole-rock compositions are reported, were sampled by drill. We sampled virtually every fresh outcrop in the ~160 km^2 area of the Chugwater Anorthosite; gaps in our sample base are not for want of trying!

The Chugwater Anorthosite is characterized by distinctive layering, both modal and textural, foliation of tabular plagioclase, which is mainly parallel to the layering, presence of tabular and megacrystic plagioclase, much of which shows labradorescence and is typically deformed to varying degrees, and a distinctive magmatic stratigraphy in its western portion. It shares some of these characteristics with each of the nearby Poe Mountain and Snow Creek anorthosites, but is distinctive in its totality. Both Snow Creek and Chugwater anorthosites have abundant labradorescent plagioclase (~$An_{52–57}Or_{3–4}$); the Poe Mountain Anorthosite is mainly too sodic to show that feature. Both the Poe Mountain and Chugwater anorthosites have both titaniferous magnetite and ilmenite, whereas the Snow Creek lacks magnetite but has ilmenite, typically with inclusions of rutile.

In this paper, we present field, petrographic, and geochemical evidence that leads us to conclude that the Chugwater Anorthosite is a layered feldspathic intrusion that was emplaced at approximately 10–12 km depth by injection of several major pulses (at least three) of magma laden with plagioclase crystals (probably 40% crystals of ~An_{52}). The silica activity of these magmas was high (0.7 to 1.0 relative to quartz), and thus the main Chugwater Anorthosite is olivine-free. This main series was repeatedly intruded by, and locally mixed with, at least two different leucotroctolitic magmas, one having normative An very close to that of the

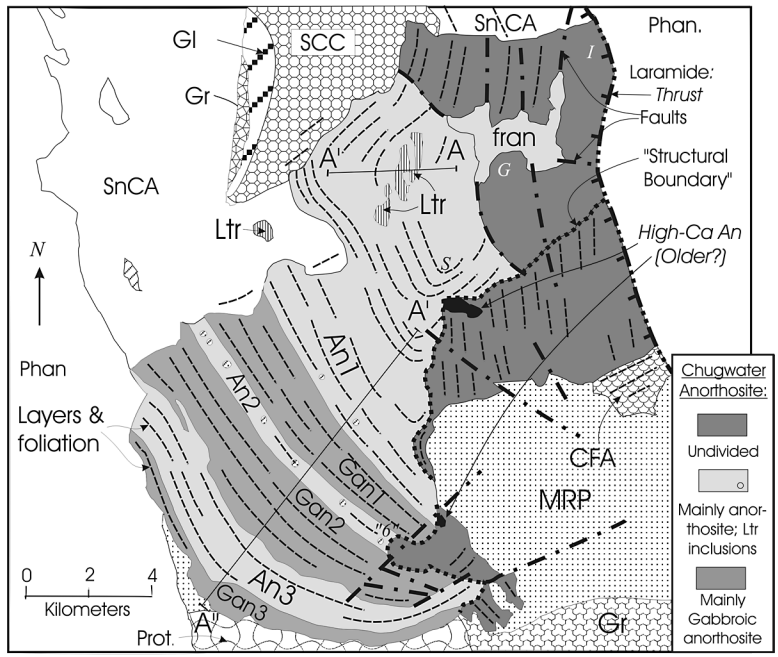

FIG. 2. Geological map of the Chugwater Anorthosite and surrounding rocks. Thick dashed lines show the strike of layering and foliation. The central and southwestern portions of the Chugwater Anorthosite have well-constrained stratigraphic relations and are called the "Stratigraphic Chugwater Anorthosite". That stratigraphy has been constructed across the lines A–A' and A'–A''; thicknesses have not been measured directly, but are estimated from dip and horizontal extent. East of the "structural boundary", the Chugwater Anorthosite has a distinctly different foliation, and stratigraphic positions cannot be assigned. Similarly, the Chugwater Anorthosite to the northeast is cut by numerous faults of Laramide age (only the most prominent are shown) and by granitic dikes; accordingly it was not possible to assign stratigraphic positions to this portion as well. The high-Ca anorthosites are the largest of numerous inclusions of high-An anorthosite that decorate the "structural boundary" within the Chugwater Anorthosite, as well as parts of its boundary between with the Maloin Ranch Pluton. Abbreviations: GI: Greaser intrusion, SnCA: eastern portion of Snow Creek Anorthosite, SCC: Strong Creek Complex, CFA: Coyote Flats Anorthosite, Ltr: leucotroctolite intrusions (only the largest are shown), fran: fractured anorthosite of Newhouse & Hagner (1957), Gr: granite, including the Mule Creek lobe (northern portion) and Sherman Granite (southern portion). Locations of major Fe–Ti oxide deposits are given by *I*: Iron Mountain, *G*: Goat Mountain, *S*: Shanton.

main-series anorthosite, the other distinctly more calcic (normative $An_{58–64}$). The mixed rocks show normative and modal olivine. There is an overall upward increase of incompatible trace elements, suggesting that there was at least some communication of residual melts throughout the intrusion.

Layering, Stratigraphy, and Structure

Layering: size and morphology of plagioclase

By definition, anorthosites contain 90% or more modal plagioclase. Because many of the features of the Chugwater Anorthosite to be described reflect the nature of its plagioclase, it is useful to provide an overview, with details to follow in the petrography section. Somewhat arbitrarily, we call tabular grains wider than approximately 5 cm *megacrysts*. Typical megacrysts range up to 10 cm in width, but larger ones occur as well. Outcrops with abundant, oriented megacrysts glint brightly in sunlight, earning the field name "silver-dollar anorthosite". We argue in a later section that the megacrysts and some but not all of the smaller tabular plagioclase were present in the magmas when the Chugwater Anorthosite was emplaced.

The Chugwater Anorthosite is layered on scales that range from centimeters to kilometers. Much layering reflects variations in modal abundance of plagioclase relative to ferromagnesian minerals (Figs. 3a, b); typically the range is from approximately 85 to 96% plagioclase. Rarely can layers be traced over distances greater than 10–20 times their thickness. Some terminate abruptly, but most die out gradually, as along-strike variations in mode diminish the difference between adjacent layers. In addition to anorthosite and gabbroic anorthosite, the Chugwater Anorthosite contains numerous bodies of troctolite and leucotroctolite. The larger bodies cross-cut the anorthositic units, but smaller ones (dimensions from a few meters to several tens of meters) typically lie parallel or subparallel to the regional layering. Boundaries tend to be sharp where leucotroctolite cuts anorthosite, but more diffuse against gabbroic anorthosite.

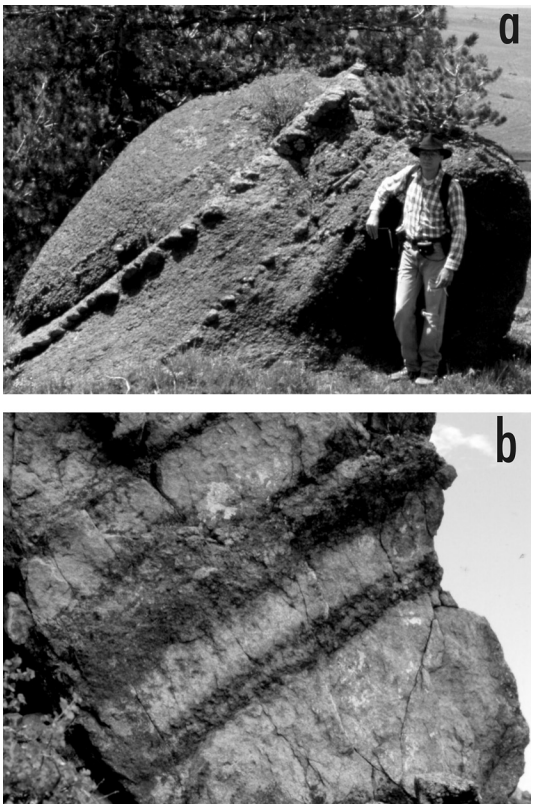

FIG. 3. Photographs showing compositional layering in the Chugwater Anorthosite. a. Thin layers of anorthosite (weathers in relief) in gabbroic anorthosite. The geologist is 1.8 m tall. b. Layers of gabbroic anorthosite (dark) in anorthosite (light). The lowest dark layer is approximately 15 cm thick.

Lamination resulting from the subparallel alignment of tabular and megacrystic plagioclase produces a foliation that is nearly always parallel to compositional layering. Although we have not made a detailed study in the Chugwater Anorthosite, we infer that there is no orientation of plagioclase *within* the foliation and thus no lineation, similar to the findings of Lafrance *et al.* (1996) for the Poe Mountain Anorthosite. Textural layering is also mainly parallel to modal layering and plagioclase lamination, and can take several forms. Most commonly it is expressed by variations in grain size, usually of plagioclase, and thus may complement modal layering. But textural layering also reflects across-strike variations in the degree of deformation through grain-boundary migration in plagioclase. Typically, the most plagioclase-rich layers show the greatest deformation, expressed by the presence of bent twins and abundant neoblastic recrystallized plagioclase. Such layers typically range from centimeters to tens of meters in thickness, and like modal layers, rarely can be traced for distances greater than 10–20 times their thickness; many contain angular relics of megacrysts.

Stratigraphy

We call the western portions the "stratigraphic Chugwater Anorthosite", because the largest-scale layers (Figs. 2, 4) define a distinctive stratigraphy consisting of three dominantly anorthosite units (from base to top, An1, An2, An3) and three slightly more mafic units with 80–90% plagioclase. According to Streckeisen (1967), the more mafic units are leucogabbros. However, to emphasize their close affinity with the true anorthosites of the Chugwater Anorthosite, we here follow Buddington (1939) and call them gabbroic anorthosites, a term also accepted by Streckeisen (1976). An advantage of this usage is that "anorthositic" can then be used as a general term for the entire series. We call the more mafic units the lower, middle, and upper gabbroic anorthosites (Gan1, Gan2, Gan3), respectively. Each pair (*e.g.,* An1 + Gan1) is considered a magmatic unit, so the three pairs comprise Units 1, 2, and 3. Critical sample localities are given in Figure 4. We emphasize that each of these stratigraphic units contains compositional layering on successively finer scales, so that it is common to find true anorthosite within each of the gabbroic anorthosite units and *vice versa*. A composite section (A–A' and A'A'' in Fig. 2) totals just over 10,000 m (Fig. 5). We are confident regarding the top 8000 m of section; the need to correlate nearly 5 km along strike across possible offsets by Laramide-age faults, combined with gentler dips, make the lower 2000 m of the section somewhat less certain. Furthermore, the base for the section is arbitrarily chosen near the trace of prominent Laramide faults; more anorthosite outcrops to the east (*i.e.,* below the base chosen for the stratigraphic Chugwater Anorthosite), but a combination of

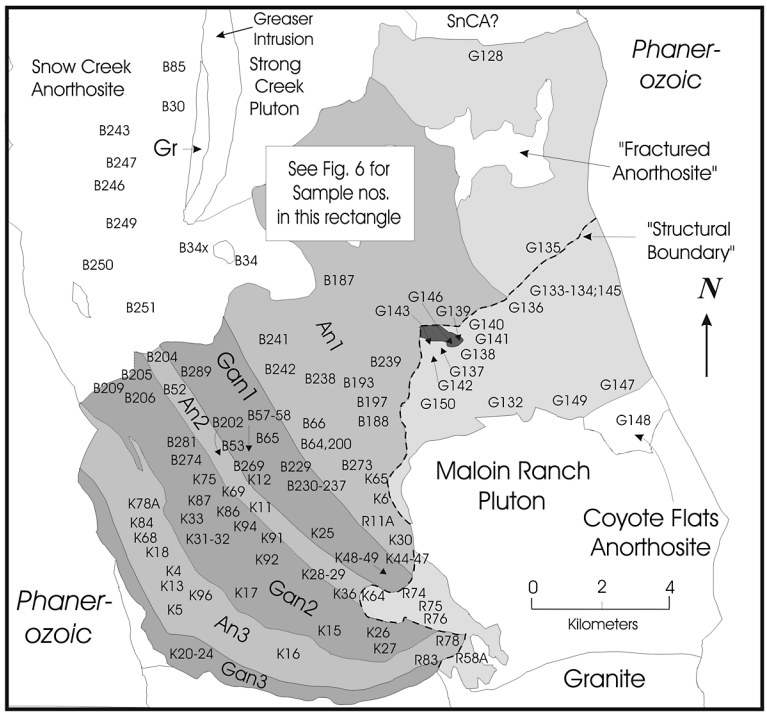

FIG. 4. Sample-location map for the Chugwater Anorthosite and nearby rocks. Sample locations not shown on this map are indicated in Figures 1 and 6. To save space, quadrangle designators are abbreviated: B: BM (Baldy Mountain), G: GM (Goat Mountain), K: KM (King Mountain), R: RTM (Ragged Top Mountain).

poor exposure, late-magmatic alteration, and extensive Laramide faulting in that area preclude stratigraphic assignment in this region (Fig. 2), so we exclude it from the stratigraphic Chugwater Anorthosite. We emphasize that the stratigraphic section has not been measured directly, but has been constructed using map distances and average dips in each area.

Unit An1 (0–4750 m; Fig. 2) is the thickest and least well defined of the units. In addition to the uncertainties in correlation mentioned above, it is cut by several large leucotroctolite bodies (Fig. 6). Unit Gan1 (4750–5590 m) locally contains the best modal layering on the 10–100 cm scale, but its generally subdued topography yields few good outcrops. Unit An2 (5590–6240 m) is the thinnest of the main units; it stands out clearly on satellite images and as local highs on topographic maps. It also contains a distinctive series of leucotroctolite pods, 2 to 20 m across, that occur throughout its exposed length of nearly 10 km. Gan2 (6240–8300 m) is the thickest of the gabbroic anorthosite units. An3 (8300–9520 m), the uppermost anorthosite, is the most distinctive of the six units: it consists almost entirely of extremely well-laminated medium-grained (typically 2–3 cm across, 2–3 mm thick) tabular anorthosite. It ranges in thickness from 700 meters in the southeast to 1220 m in the vicinity of King Mountain (section 3, T17N, R72W). Megacrysts, although present, are much rarer than in lower units. Similar medium-grained tabular anorthosite also occurs locally 4000 m lower, near the top of An1, but typical thicknesses there are 1–5 meters, and these layers cannot be traced more than 100 m along strike. The topmost unit, Gan3 (9520–10,400 m), is irregular in thickness, ending against country rock to the south and being truncated by a poorly exposed monzosyenite unit to the southwest. The sequence described here stands in contrast to the layered units of Michikamau Intrusion, Labrador (Emslie 1970), where anorthosite overlies more mafic layers, a relationship to be expected if buoyancy alone controlled the formation of layering. John Longhi (written commun., 2009) has suggested the possibility that our Gan1 might more logically be paired with An2, and Gan2 with An3. Unfortunately, none of our data, field, petrographic, or geochemical, permits us to test that idea. We retain our field-based pairings in part by analogy with the nearby Poe Mountain Anorthosite, where more mafic

layers clearly overlie more anorthositic units despite the expectation that plagioclase would be buoyant. Scoates (2000, 2002) has addressed this "plagioclase – magma density paradox" for the Poe Mountain Anorthosite.

Structure

The well-developed layering and foliation of the Chugwater Anorthosite make it possible to define several structural features. The stratigraphic Chugwater Anorthosite consistently dips to the west and southwest,

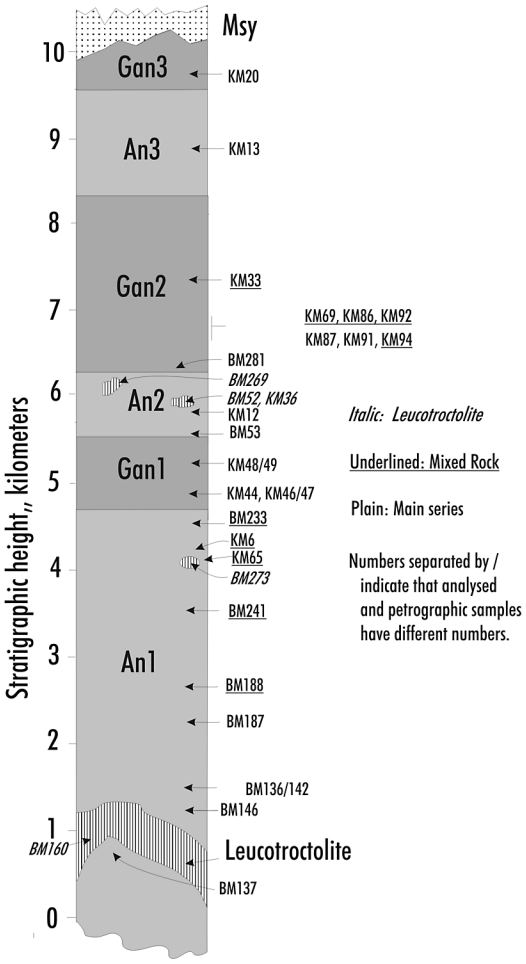

FIG. 5. Stratigraphic column for the southwestern portions of the Chugwater Anorthosite, constructed using profiles along A–A' and A'–A" in Figure 2. Some key sample numbers are shown. Light grey: units dominated by anorthosite; dark grey: units dominated by gabbroic anorthosite and mixed rocks. Vertical lines: intrusions and inclusions of leucotroctolite and troctolite. Dot pattern: monzosyenite.

with dips generally increasing up-section; it corresponds to the southwestern portion of the "anticline" proposed by Newhouse & Hagner (1957). In the eastern portions of the stratigraphic Chugwater Anorthosite, we do in fact see some hints of an "anticlinal axis" (central portion of Fig. 2). However, the details are considerably more complicated. To the west and north of the Maloin Ranch Pluton (thus close to the "anticlinal axis" of Newhouse & Hagner), there are abrupt discontinuities in structure between the stratigraphic Chugwater Anorthosite and very similar anorthosites lying to the east and southeast (Fig. 2). The discontinuities in strike are evident on the map, but the dips are discordant as well: most of the dips in the nearby stratigraphic Chugwater Anorthosite are 30° or less, whereas those of the north–south striking anorthosites to the east are all greater, with most being at least 70°. We define the region of abrupt structural change as a "structural boundary". In a number of places, this boundary is decorated by inclusions of highly deformed anorthosite that is much more calcic ($An_{67–75}$) than the Chugwater Anorthosite. Most of these inclusions are too small to appear on Figures 2 and 6, but two larger inclusions are shown. In the southeastern Chugwater Anorthosite, the "structural boundary" separates rocks on the west that have distinct, consistent layering and lamination from ones on the east where such features are either lacking or chaotic. Petrographically and compositionally, there are no differences between the rocks on either side of the "structural boundary", so we consider them all to be parts of the Chugwater Anorthosite. Evidently, they have experienced distinctly different deformational histories. It is noteworthy that with the exception of the inclusions noted above, none of the Chugwater Anorthosite shows the highly deformed and granulated rocks seen at the borders of the Egersund–Ogna anorthosite, Norway (Barnichon *et al.* 1999), and similar plutons believed to have been emplaced diapirically.

Laramide faulting. The Chugwater Anorthosite, in common with most of the LAC, has been cut by numerous faults and shear zones of presumed Laramide age. In general, these increase in abundance from west to east, and, indeed, the northeasternmost portion of the Chugwater Anorthosite has been thrust eastward over Phanerozoic limestones, some of which have been locally overturned. In most places within the anorthosite, it is impossible to determine either the direction or extent of displacement along the other faults. Proterozoic granite dikes showing little or no offset suggest that many of these features may have been shear zones with little displacement. In any event, they make it extremely difficult to trace layers and other structures in the northeastern portion of the Chugwater Anorthosite. This is the major reason that we arbitrarily start the base of the "stratigraphic Chugwater Anorthosite" west of the region of abundant faults. Just to the east of the region of Figure 6 (see Fig. 4), so many of these features intersect that the anorthosite was highly comminuted

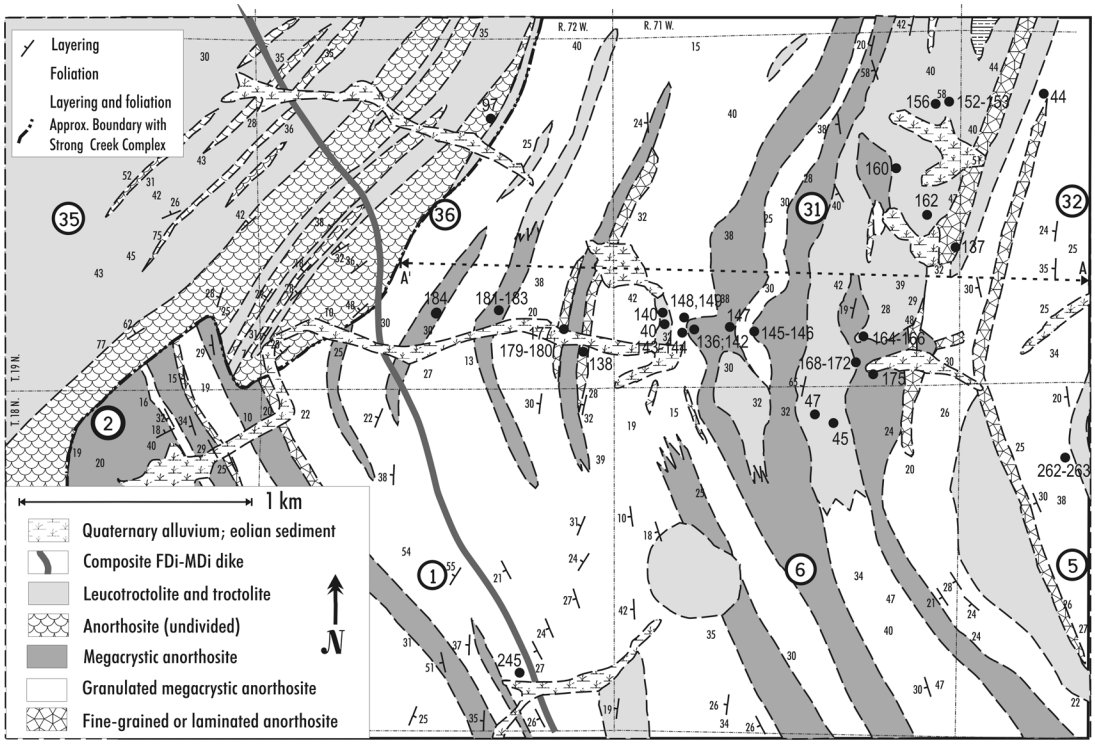

FIG. 6. Detailed geological map of the lower portions of the stratigraphic Chugwater Anorthosite (shown as rectangle in Fig. 4). Locations of samples are indicated by sample numbers; the prefix BM has been omitted. Sample locations shown here are omitted from Figure 4. FDi: ferrodiorite, Mdi: monzodiorite (see also Mitchell *et al*. 1996, Fig. 2). Dip and strike symbols show the orientation of compositional layering and of plagioclase orientation. Dashed line shows the position of profile A–A' (Fig. 2). Horizontal and vertical dot-dash lines are section boundaries; section numbers are shown within circles. Township and range data are from the U.S. Geological Survey Baldy Mountain Quadrangle topographic map, 7.5 minute series, 1955, photorevised 1981.

and has been preferentially weathered and eroded. We have retained the term of Newhouse & Hagner (1957) "fractured anorthosite" (fran) for this area.

Possibility of a detachment thrust beneath the Chugwater Anorthosite. Geophysical measurements, both gravity (Hodge *et al*. 1970, 1973, Smith *et al*. 1970) and seismic reflection (Allmendinger *et al*. 1982, Brewer *et al*. 1982), consistently show that the anorthosite bodies in the LAC at present are quite thin (1.6 to 4 km) compared to their areal extent (~650 km^2) and inferred stratigraphic thickness. This is most surprising in view of the fact that stratigraphic thicknesses of 6000–10,000 m have been documented in both the northern (Poe Mountain Anorthosite: Scoates 1994, Scoates *et al*. 2010) and southern (Chugwater Anorthosite; this paper) portions of the LAC. One possible explanation is that the present exposures of the LAC lie above a Laramide detachment thrust. Besides the geophysical studies, the only evidence for this interpretation is a report that a diamond-drill hole at Iron Mountain (*I* in Fig. 2) penetrated Paleozoic limestone (pers. commun. from Donald L. Blackstone to B.R. Frost).

Significance of the "anticlinal axis" of Newhouse & Hagner. Our mapping in the Chugwater Anorthosite shows that the "anticlinal axis" reported in the area by Newhouse & Hagner (1957) actually reflects the combination of two and possibly three distinct features: (1) the very real and regular westerly to southwesterly dip of the stratigraphic Chugwater Anorthosite, together with local curvature in the southern and central portions of Figure 4, and (2) the abrupt change to mainly north–south-striking, nearly vertical fabric to the east and south of the "structural boundary". In addition, there is the very real possibility, especially near the eastern boundary thrust, that disparate portions of the Chugwater Anorthosite may have been juxtaposed by Laramide-age faulting, and that any appearance of an antiform there may be accidental and therefore misleading.

Granites and other dikes

The Chugwater Anorthosite is cut by a variety of granitic dikes, none of which is large enough to show on the scale of Figures 1 and 2. Their thickness is variable, ranging from 1 to 15 m. Most of these dikes strike N–S to NW–SE, although all other orientations occur. In general, both the size and abundance of these dikes increase from west to east. Some dikes have negligible effects on the host anorthosite and were probably relatively dry. Other dikes, probably with high H_2O contents, pervasively altered the anorthosite through which they passed: the plagioclase is bleached white, whereas the ferromagnesian minerals have been converted to hornblende or actinolite. Some dikes alter the anorthosite to distances ten times their own thickness. The concentration of such alteration in the eastern portions of the Chugwater Anorthosite adds greatly to the difficulty in recognizing and tracing stratigraphic variations in that area. Together with the greater effects of Laramide faulting in the east, this led us to concentrate our efforts in the more tractable western parts of the Chugwater Anorthosite ("stratigraphic Chugwater Anorthosite"). A composite ferrodiorite–monzodiorite dike (Mitchell 1993) cuts part of the Chugwater Anorthosite (Fig. 6). Smaller dikes of ferrodiorite also occur.

Fe–Ti oxide bodies

The Chugwater Anorthosite is host to four deposits of massive Fe–Ti oxides; from northeast to southwest, these are the well-known Iron Mountain deposit (Hayden 1871, Ball 1907, Singewald 1913, Frey 1946a, Eberle 1983), the Goat Mountain prospect, the Shanton deposit (Hild 1953, Frey 1946b), and an unnamed prospect in section 6, T17N, R71W (I, G, S, and "6" in Fig. 2). Newhouse & Hagner (1957) noted that these all lie on or adjacent to their "anticlinal axis". Our more detailed mapping raises serious doubts regarding this apparent correlation.

Petrography and Mineral Compositions

Analytical

Mineral compositions were determined by electron-probe microanalysis. Most analyses were made on the Stony Brook Cameca "Camebax" probe, using an accelerating potential of 15 kV and sample currents of 15 nA for plagioclase and 20 nA for other phases. We used, as standards for plagioclase, microcline for K, albite for Na, anorthite for Ca, Al, and Si, ilmenite for Ti, and fayalite for Fe. For ferromagnesian phases, we used enstatite for Mg and Si, anorthite for Ca and Al, ilmenite for Ti, fayalite for Fe, except hematite for Fe in Fe–Ti oxides, and rhodonite for Mn. Some ferromagnesian and oxide minerals were measured at the University of Wyoming using 15 kV and 20 nA and the following standards: for augite, Si, Al, Ti, Mg, Fe, Na, and Ca on augite, Cr on chromite, Ni on synthetic Ni-olivine, Mn on magnesian fayalite. For orthopyroxene, we used Si, Mg, Fe on ferroan enstatite, Al, Ti, Ca, and Na on augite, Cr on chromite, Ni on synthetic Ni-olivine, Mn on magnesian fayalite. For olivine, we used Si, Fe, and Mn on magnesian fayalite, Mg on ferroan enstatite, Al, Ti, and Ca on hornblende, Cr on chromite, Ni on synthetic Ni-olivine. For ilmenite, we used Fe, Ti, and O on ilmenite, Mn on magnesian fayalite, Mg, Al, and Cr on a chromium-rich ulvöspinel, and Zn on gahnite.

Textures

The dominant feature of almost all samples of anorthosite and gabbroic anorthosite in the Chugwater Anorthosite is the presence of plagioclase megacrysts. In preparing samples for thin-sectioning, one must be careful to ensure that phases other than plagioclase are present on the surface chosen. One result of this selection process is that point-counted modes are nearly meaningless, as they tend to underestimate the true volume of plagioclase in the sample. In the Poe Mountain Anorthosite, poikilitic textures (with augite, orthopyroxene, olivine, and even Fe–Ti oxides all serving as oikocrysts) are common, suggesting simultaneous crystallization of those phases and plagioclase (Scoates 1994, Scoates *et al.* 2010). In contrast, a poikilitic texture is extremely rare in the Chugwater Anorthosite; all ferromagnesian phases are interstitial to plagioclase, suggesting that they formed only after the majority of plagioclase had already crystallized. The Chugwater Anorthosite textures are consistent with the body having been emplaced as a magma laden with plagioclase crystals. In Table 1, we list the minerals present and the range of plagioclase compositions for key samples of the Chugwater Anorthosite. Available average compositions of plagioclase, clinopyroxene, orthopyroxene, and olivine are given in Tables 2a – 2d.

Overview of mineralogy

Plagioclase. The single most distinctive feature of the Chugwater Anorthosite is its abundant coarse, tabular plagioclase, much of which shows labradorescence. The tabular face is [010], with the larger axes subequal, and the thickness distinctly less than that of the other dimensions. Rarely are faces other than [010] preserved. Typically tabular grains up to ~5 cm across have thicknesses of 0.5 cm or less. Megacrysts (tabular plagioclase with widths greater than 5 cm) typically have proportionally greater thicknesses, of the order of 0.2× the width. Plagioclase compositions in most of the Chugwater Anorthosite and some of the leucotroctolites are typically An_{50} to An_{56}; whereas the *range* of compositions in a given sample increases toward the top

of the stratigraphic section, overall there appears to be a 1–2% upward decrease in An content (Figs. 7a, b, c). The most common composition is $An_{52–54}Or_{3–4}$, which leads to iridescence in the blue to blue-green range. Many anorthosite samples contain a few plagioclase grains that are distinctly more calcic than the rest. We interpret these as xenocrysts, probably from the older calcic anorthosites that are found as inclusions within parts of the Chugwater Anorthosite. Two sets of leucotroctolites, at the 5960–6075 m and 9740 m levels, are also distinctly more calcic (Fig. 7c). Some calcic plagioclase in the Chugwater Anorthosite may reflect mixing between these leucotroctolites and the host anorthositic units (to be discussed later).

Deformation. Nearly all plagioclase in the Chugwater Anorthosite shows varying extents of deformation, most of it high-temperature. In the least-deformed rocks, megacrystic and other tabular plagioclase grains have sutured grain-boundaries and are bent, as can be seen both in hand sample and in thin section (Figs. 8a–c). As the extent of deformation increases, the tabular grains may become polygonalized, and neoblasts form on their grain boundaries, a process documented by Lafrance *et al*. (1996). The neoblasts lack the Fe–Ti oxide inclusions that give the megacrysts their distinctive black color. As the population of neoblasts increases, the relict megacrysts remain as black porphyroclasts isolated by gray to white neoblasts.

TABLE 1. MODAL MINERALOGY OF KEY SAMPLES FROM THE CHUGWATER ANORTHOSITE

Sample	Height m	Unit, Rock	% Pl	An Norm	Min An	Max An	Modal An	Ol	Opx	Pgt	Aug	Bt	Ilm	Mgt
Main series														
BM137	688	An1, An	95.2	54.8	53	73	54-56				1			
BM146	1243	An1, An	95.0	54.5	n.d.	n.d.	n.d.				2	1	2	1
BM136,142	1404	An1, An	94.5	54.1	51	59	52-54				1	1	1	2
BM187	2180	An1, An	96.6	54.8	52	54	52-54				1	1	2	
BM238	3005	An1, An	96.4	55.3	52	58	53-54							
KM044,45	4900	Gan1, An	93.1	53.8	n.d.	n.d.	n.d.		1		3	2	2	2
KM046,47	4900	Gan1, An	94.9	53.6	48	54	49-53		2		2	1	1	1
KM049,48	5200	Gan1, An	92.4	54.2	n.d.	n.d.	n.d.		2		2	2	2	
BM053	5600	Gan1, Gan	91.9	55.2	50	56	51-54		1		2		2	1
KM012	5850	An2, An	90.6	54.1	51	54	52-53		2		2		2	2
BM281	6245	Gan2, Gan	85.1	54.4	n.d.	n.d.	n.d.				2	1	1	2
KM091	6790	Gan2, An	91.3	53.4	n.d.	n.d.	n.d.		1		2		1	2
KM013	8860	An3, An	92.6	54.5	n.d.	n.d.	n.d.						2	
KM020	9740	Gan3, Gan	80.1	51.6	47	57	49-54		1	3	2	1	1	
Mixed Rocks														
BM241	3550	An1, Mix	85.5	53.6	50	53	50-51	1	2		3	2	2	2
KM065	4180	An1, Mix	92.9	53.9	51	55	52-55	1	2		2	1	1	1
KM006	4250	An1, Mix	83.9	54.7	47	52	48-51	2	3		3	2	1	2
BM233	4630	Gan1, Mix	89.1	55.0	n.d.	n.d.	n.d.	1	3		2	2	1	
KM094	6525	Gan2, Mix	88.2	55.3	n.d.	n.d.	n.d.	1	3		2	1	2	2
KM069	6615	Gan2, Mix	85.2	55.4	48	54	49-53	3	2		2	1	2	1
KM087	6715	Gan2, Mix	92.4	52.7	n.d.	n.d.	n.d.		1		2		2	2
KM092	6785	Gan2, Mix	88.7	54.8	49	53	51-53	3	1		2		1	1
KM086	6895	Gan2, Mix	84.6	53.8	52	55	52-55		2		2	1	2	2
KM033	7256	Gan2, Mix	85.0	55	50	57	50-54	3	1		2	2	1	2
Troctolite and Leucotroctolites														
BM160	863	An1, Lt	70.6	54.2	50	52	51-52	3	2		2	2	1	2
BM273	4180	An1, Tr	63.1	56.1	47	74	49-54	3	2		2	2	2	2
KM036	5960	An2, Lt	70.6	58.8	55	61	58-60	3	2		2	2	1	
BM052	6000	An2, Lt	89.0	63.8	60	64	61-64	2	2		3		1	1
BM269	6075	An2, Lt	83.5	61.2	58	74	60-65	3	2		2	1	1	

Notes: Height: stratigraphic height (meters) above an arbitrary base. Units: (An1, An2, Gan2, *etc.*) indicate the dominant lithology (Anorthosite, >90% Pl; Gabbroic anorthosite, 80–90% Pl) shown in Figures 2, 4, and 5. Rock is the lithology of the actual sample; Lt: leucotroctolite, Tr: troctolite. %Pl is the total normative feldspar; in most cases, this agrees well with visual estimates of modal plagioclase. An Norm is the normative An/(An+Ab+Or). Min, Max, and Modal An are the highest, lowest, and most abundant compositions determined by electron microprobe. Abundances of ferromagnesian minerals are relative only: 1 means at least one grain present, 2 means at least five grains, and 3 indicates "highly abundant", with the reminder that most thin sections contain at least 80% plagioclase! Mgt is titaniferous magnetite, typically a low-Ti magnetite host containing ilmenite lamellae in {111}. n.d.: not determined.

TABLE 2a. PLAGIOCLASE COMPOSITIONS IN THE CHUGWATER ANORTHOSITE

	Main series											
Sample	BM137	BM142	BM187	BM238	KM047	BM053	KM012	BM205	KM017	KM018	KM004	KM020
Height, m	688	1404	2180	3005	4900	5600	5850	6295	8050	8500	8750	9740
SiO_2 wt%	53.66	54.27	55.35	54.94	53.98	54.94	55.27	54.92	55.31	54.55	55.18	55.62
TiO_2	0.06	0.02	0.04	0.04	0.02	0.07	0.05	0.04	0.09	0.03	0.02	0.06
Al_2O_3	28.99	28.59	28.43	28.63	27.91	28.20	28.24	28.18	28.32	28.96	28.77	28.31
Fe_2O_3(T)	0.25	0.25	0.16	0.26	0.21	0.30	0.35	0.26	0.20	0.25	0.24	0.23
CaO	11.40	11.03	10.82	11.10	10.29	10.97	10.85	10.71	10.76	11.65	11.21	10.93
Na_2O	4.99	5.04	5.27	5.19	5.13	4.90	5.11	4.93	5.27	4.87	5.14	5.23
K_2O	0.18	0.44	0.19	0.31	0.41	0.59	0.45	0.54	0.39	0.32	0.28	0.46
Sum	99.53	99.62	100.26	100.46	97.95	99.97	100.32	99.58	100.34	100.63	100.85	100.83
#	9	12	9	20	23	12	8	6	8	8	8	8

	Mixed rocks									Troctolite and leucotroctolite				
Sample	BM157	BM188	BM241	KM065	KM006	KM069	KM092	KM086	KM033	BM160	BM273	KM036	BM052	BM269
Height, m	760	2680	3550	4180	4250	6615	6785	6895	7255	863	4180	5960	6000	6075
SiO_2 wt%	54.89	55.21	55.75	55.03	55.92	54.25	54.85	55.01	54.63	54.43	53.21	53.56	52.19	51.65
TiO_2	0.08	0.06	0.07	0.11	0.08	0.08	0.08	0.05	0.06	0.04	0.04	0.07	0.03	0.07
Al_2O_3	28.30	28.07	28.30	28.22	28.11	28.29	28.18	27.99	28.38	28.42	28.07	29.26	30.11	30.05
Fe_2O_3(T)	0.23	0.25	0.23	0.63	0.20	0.19	0.23	0.27	0.26	0.22	1.03	0.14	0.25	0.29
CaO	10.99	10.57	10.63	10.90	10.34	10.18	10.55	10.80	10.69	10.61	10.57	11.71	12.58	12.86
Na_2O	4.95	4.98	5.26	4.94	5.30	5.18	4.99	4.86	5.12	5.39	5.09	4.46	4.05	3.94
K_2O	0.38	0.60	0.64	0.58	0.62	0.48	0.61	0.47	0.67	0.56	0.31	0.43	0.34	0.27
Sum	99.81	99.73	100.89	100.41	100.57	98.64	99.49	99.45	99.81	99.68	98.31	99.63	99.54	99.13
#	6	15	8	9	8	29	6	6	15	10	30	6	12	10

#: average result of # electron-microprobe analyses.

Where most of the original plagioclase has recrystallized, the result is a fine-grained white to gray rock with a granoblastic texture. Even in the most recrystallized rocks, however, one may find local black, iridescent fragments of the original magmatic plagioclase.

Inclusions in plagioclase. All megacrysts and most other tabular plagioclase grains in the Chugwater Anorthosite are dark grey to black as the result of numerous inclusions (Fig. 8a). There are two main types of inclusions, both of which are oriented in preferred directions: black opaque rods (mainly magnetite and ilmenite) and honey-colored to red-brown plates that are rich in Ti and Fe (mainly ilmenite and rutile, but with some biotite). Many of the plates are so thin (<1 μm) that they are non-opaque (Fig. 8d). Plagioclase with the inclusions typically contains 0.3–0.4 wt% TiO_2. Both types of inclusions are absent from plagioclase of the cross-cutting troctolites and leucotroctolites. They are also absent from neoblastic plagioclase and from rims on megacrysts. In a later section, we suggest that the inclusion-bearing regions may indicate crystals that formed at greater depth and were present when the Chugwater Anorthosite magma was emplaced.

Pyroxenes. Some pyroxene grains in gabbroic anorthosite are subhedral, suggesting that they may be cumulus; most, however, are clearly interstitial to plagioclase, as is always the case for anorthosite units. Oikocrystic pyroxene, common in the Poe Mountain Anorthosite to the north (Scoates 1994, Scoates *et al*. 2010), is essentially absent in the Chugwater Anorthosite.

Augite is the most common pyroxene in the Chugwater Anorthosite. Typically, it has exsolution lamellae of low-Ca pyroxene and of ilmenite. In the leucotroctolites, it has the composition $Wo_{40}En_{45}Fs_{15}$. Augite from the gabbroic anorthosites is somewhat more iron-rich, in the range $Wo_{40}En_{40–44}Fs_{16–20}$, and that from the olivine-free (main series) rocks ranges from $Wo_{38}En_{40}Fs_{22}$ to $Wo_{40}En_{34}Fs_{26}$ (Fig. 9). The augite contains only minor non-quadrilateral components. The amount of Al_2O_3 ranges from 2.0 to 3.5 wt%, TiO_2, from 0.4 to 0.9 wt% and Na_2O, from 0.3 to 0.4 wt%. Augite from the leuc-

TABLE 2b. CLINOPYROXENE COMPOSITIONS IN THE CHUGWATER ANORTHOSITE

	Main series						Mixed Rocks				Troctolite and leucotroctolites			
Sample	M033	BM053	BM142	BM137	KM020	KM020	KM065	KM086	KM092	KM094	BM160	BM273	KM036	BM269
Height, m	688	1404	5600	7255	9740	9740	4180	6525	6785	6895	863	4180	5960	6075
SiO_2 wt%	50.83	50.48	50.82	50.65	50.92	50.16	50.49	50.53	50.78	50.90	51.91	51.19	50.99	51.74
TiO_2	0.50	0.56	0.50	0.63	0.39	0.24	0.65	0.71	0.66	0.39	0.53	0.42	0.92	0.44
Al_2O_3	2.44	2.47	2.34	2.55	1.57	0.81	3.03	3.09	3.14	1.96	3.09	2.76	3.39	2.46
FeO	11.68	11.69	13.12	10.16	13.49	26.91	10.04	10.18	9.93	13.54	10.09	11.43	8.56	13.74
MnO	0.24	0.31	0.28	0.24	0.30	0.54	0.24	0.23	0.20	0.34	0.17	0.24	0.19	0.30
MgO	11.24	12.24	14.06	12.99	11.68	16.15	13.10	13.36	13.68	12.15	15.67	16.69	14.46	18.54
CaO	21.50	20.35	18.01	20.33	20.56	4.07	21.02	20.55	20.60	19.82	18.16	15.83	20.32	12.21
Na_2O	0.32	0.31	0.26	0.30	0.26	0.05	0.37	0.38	0.38	0.26	0.29	0.29	0.36	0.22
Total	98.75	98.42	99.46	97.80	99.17	98.93	99.00	99.09	99.38	99.42	99.91	98.96	99.33	99.71
Si *apfu*	1.942	1.931	1.926	1.938	1.953	1.960	1.913	1.911	1.911	1.944	1.924	1.921	1.906	1.925
Ti	0.014	0.016	0.014	0.018	0.011	0.007	0.019	0.020	0.019	0.011	0.015	0.012	0.026	0.013
Al	0.110	0.111	0.105	0.115	0.071	0.037	0.135	0.138	0.139	0.088	0.136	0.122	0.149	0.108
Fe	0.373	0.374	0.416	0.324	0.433	0.879	0.318	0.322	0.313	0.433	0.313	0.358	0.268	0.426
Mn	0.008	0.010	0.009	0.008	0.010	0.018	0.008	0.007	0.006	0.011	0.006	0.008	0.006	0.009
Mg	0.640	0.698	0.794	0.741	0.668	0.941	0.740	0.753	0.767	0.692	0.865	0.932	0.806	1.026
Ca	0.880	0.834	0.733	0.833	0.845	0.176	0.853	0.833	0.831	0.811	0.723	0.638	0.814	0.490
Na	0.024	0.023	0.019	0.022	0.020	0.004	0.027	0.028	0.028	0.019	0.021	0.021	0.026	0.016
Total	3.992	3.998	4.017	3.998	4.011	4.021	4.014	4.014	4.014	4.010	4.001	4.016	4.005	4.015
fs*	0.211	0.202	0.207	0.182	0.220	0.423	0.160	0.163	0.157	0.223	0.172	0.177	0.146	0.210
en	0.362	0.392	0.446	0.415	0.364	0.479	0.429	0.435	0.445	0.382	0.487	0.526	0.462	0.567
wo	0.427	0.407	0.348	0.403	0.417	0.098	0.411	0.402	0.399	0.395	0.341	0.297	0.392	0.222
fs/(fs + en)	0.368	0.34	0.316	0.305	0.377	0.469	0.272	0.273	0.260	0.368	0.261	0.251	0.240	0.271
#	3	4	13	4	4	1	6	4	9	11	10	5	6	7

These compositions represent the average results of # electron-microprobe analyses. Cation proportions are calculated on the basis of six atoms of oxygen per formula unit (*apfu*). * Projected through the Edit window of QUILF (Andersen *et al.* 1993).

totroctolites tends to fall on the high side of the range for all these elements, whereas that from the olivine-free rocks is on the low side.

Orthopyroxene contains thin lamellae of augite along (100). Some orthopyroxene forms an overgrowth on olivine. Orthopyroxene from leucotroctolite has the composition $Wo_{1-2}En_{69}Fs_{29}$, whereas that from the gabbroic anorthosites ranges from $Wo_{1-2}En_{68}Fs_{30}$ to $Wo_{1-2}En_{60}Fs_{38}$, and that from the anorthosites, from $Wo_{1-2}En_{60}Fs_{38}$ to $Wo_{1-2}En_{51}Fs_{47}$. As with the augite, non-quadrilateral components are low, with Al_2O_3 ranging from 1.0 to 2.0 wt%, MnO, from 0.3 to 0.5 wt%, and TiO_2, from 0.2 to 0.3 wt%. Orthopyroxene from the leuctotroctolites tends to have minor-element compositions that fall on the high side of these ranges, whereas that from the main series have compositions that fall on the low side.

Although there is considerable variation (see below, Fig. 12), X_{Fe}^{Opx} [*i.e.*, Fs/(En + Fs)] for main-series rocks lies near 0.5 in the lower portions of the Chugwater Anorthosite, drops to 0.3 to 0.4 in the middle portions, and then increases fairly uniformly up to 0.56 at the top. For all leucotroctolites studied, X_{Fe}^{Opx} is equal to 0.31. As expected, X_{Fe}^{Opx} for mixed rocks lies between the values for main-series rocks and leucotroctolites at any given stratigraphic level. Even though X_{Fe}^{Opx} may be reset upon cooling (Opx gains Fe from Cpx but loses it to olivine by Fe–Mg exchange), we consider it a more reliable measure of the *mg#* of anorthositic rocks than that derived from bulk-rock analysis. [In rocks with ~90% plagioclase, small variations in the modal proportions of Fe–Ti oxides and ferromagnesian phases can make very large relative differences in bulk Mg and Fe.] Our data suggest that one may approximate the bulk *mg#* in the Chugwater Anorthosite through the relationship $mg\# = 0.92 - X_{Fe}^{Opx}$. However, that empirical relationship does *not* hold for the leucotroctolites, and it may not hold for anorthositic rocks other than the Chugwater Anorthosite.

Pigeonite is present only in the upper 2000 meters of the Chugwater Anorthosite and has "inverted" to coarse lamellae of augite broadly parallel to (001) in the orthopyroxene host. It has a bulk composition near $Wo_{10-12}En_{45}Fs_{43}$ (Fig. 9). Minor elements in the

TABLE 2c. REPRESENTATIVE ORTHOPYROXENE COMPOSITIONS IN THE CHUGWATER ANORTHOSITE

	Main series		Mixed Rocks					Troctolite, leucotroctolites		
Sample	BM053	KM020	KM065	KM069	KM092	KM086	KM033	BM273	KM036	BM0269
Height, m	5600	9740	4180	6615	6785	6895	7255	4180	5690	6075
SiO_2 wt%	51.63	50.48	52.30	52.05	52.14	50.80	50.99	52.74	53.10	52.86
TiO_2	0.19	0.14	0.17	0.24	0.22	0.17	0.23	0.15	0.29	0.19
Al_2O_3	1.24	0.60	1.58	1.44	1.58	0.89	1.40	1.79	1.76	1.60
Cr_2O_3	0.00	n.d.	0.02	0.01	0.02	0.03	n.d.	0.01	0.04	0.01
FeO	24.22	31.74	21.43	21.80	21.43	28.58	22.91	19.60	17.73	19.67
MnO	0.49	0.66	0.41	0.43	0.40	0.57	0.47	0.35	0.34	0.34
MgO	20.89	15.25	22.99	22.27	22.40	17.70	20.68	24.25	24.47	24.25
NiO	0.03	n.d.	0.02	0.01	0.03	0.03	n.d.	0.03	0.03	0.06
CaO	1.03	1.07	0.86	1.20	1.21	1.00	0.95	0.84	2.20	0.87
Na_2O	0.00	0.01	0.02	0.02	0.02	0.02	0.01	0.01	0.04	0.01
Total	99.72	99.94	99.79	99.49	99.45	99.78	97.64	99.79	100.00	99.86
Si *apfu*	1.952	1.977	1.947	1.950	1.950	1.962	1.958	1.946	1.945	1.949
Ti	0.006	0.004	0.005	0.007	0.006	0.005	0.007	0.004	0.008	0.005
Al	0.055	0.028	0.070	0.064	0.070	0.041	0.063	0.078	0.076	0.070
Cr	0.000		0.001	0.001	0.001	0.001		0.001	0.001	0.001
Fe	0.766	1.039	0.667	0.683	0.670	0.924	0.736	0.605	0.543	0.607
Mn	0.016	0.022	0.013	0.014	0.013	0.019	0.015	0.011	0.011	0.011
Mg	1.178	0.890	1.276	1.244	1.249	1.019	1.184	1.334	1.336	1.333
Ni	0.001		0.001	0.000	0.001	0.001		0.001	0.001	0.002
Ca	0.042	0.045	0.034	0.049	0.049	0.041	0.039	0.034	0.087	0.035
Na	0.000	0.000	0.002	0.002	0.002	0.002	0.000	0.001	0.003	0.001
Total	4.015	4.006	4.014	4.012	4.009	4.013	4.003	4.012	4.010	4.012
wo*	0.022	0.023	0.018	0.026	0.026	0.022	0.02	0.018	0.046	0.018
en	0.606	0.455	0.659	0.641	0.643	0.524	0.607	0.688	0.689	0.686
fs	0.372	0.522	0.323	0.334	0.331	0.455	0.372	0.295	0.265	0.296
fs/(fs + en)	0.380	0.535	0.329	0.343	0.340	0.465	0.380	0.300	0.278	0.301
#	9	2	10	12	15	12	4	15	20	5

These compositions represent the average results of # electron-microprobe analyses. Cation proportions are calculated on the basis of six atoms of oxygen per formula unit (*apfu*). * Projected through the Edit window of QUILF (Andersen *et al.* 1993).

host Opx and augite lamellae are similar to those in the primary phases. Inverted pigeonite also occurs in a small iron-enriched body that intrudes the Chugwater Anorthosite about half way up the stratigraphy.

Olivine. Olivine is absent from nearly all samples of anorthosite *sensu stricto* but is present in many gabbroic anorthosites and by definition in all leucotroctolites and troctolites. In a later section, we argue that the absence of olivine from the true anorthosites is real and significant, rather than an artifact of the low content of ferromagnesian minerals in these rocks. Olivine has a composition near Fo_{65} in the leucotroctolites and troctolites and ranges from Fo_{65} to Fo_{54} in the olivine-bearing gabbroic anorthosites (Fig. 9). The CaO, MnO, and NiO contents of olivine are low, less than 0.03, 0.5, and 0.2 wt%, respectively. In approximately half our samples, olivine has partially or completely altered to chlorite plus other phases.

Biotite. Biotite typically makes up 1–2 vol.% of leucotroctolites, occurs in some gabbroic anorthosites (typically those containing olivine), and is absent from anorthosites (except as occasional oriented lamellae in plagioclase megacrysts). It typically rims Fe–Ti oxide and has the deep-red color associated with elevated content of Ti.

Quartz. Primary quartz is absent from the leucotroctolites and most of the Chugwater Anorthosite. Most samples that contain inverted pigeonite in the uppermost 2000 m of the Chugwater Anorthosite also contain trace to minor amounts of primary quartz.

Fe–Ti oxide. Both the Chugwater Anorthosite and the associated leucotroctolites contain ilmenite and titaniferous magnetite (Ti–Mgt). Typically, the latter is more abundant, appearing as grains and (111) lamellae of ilmenite in a relatively low-Ti magnetite host. Rarely, is it possible to reconstruct the original spinel composition by re-integrating the oxy-"exsolved" lamellae with the host; QUILF calculations (see a later section) suggest original compositions of $Usp_{40–60}$. In rocks where titaniferous magnetite dominates, the ilmenite is

TABLE 2d. OLIVINE COMPOSITIONS IN THE CHUGWATER ANORTHOSITE

	Mixed rocks							Troctolite, leucotroctolites			
Sample	BM188	BM241	KM065	KM006	KM069	KM092	KM033	BM160	BM273	KM036	BM269
Height, m	2680	3550	4180	4250	6615	6785	7255	863	4180	5960	6075
SiO_2 wt%	35.13	35.38	35.84	34.81	36.23	35.98	34.39	36.65	36.46	36.83	36.53
TiO_2	0.01	0.01	0.01	0.01	0.01	0.01	0.02	0.00	0.01	0.01	0.00
Al_2O_3	0.00	0.00	0.00	0.01	0.00	0.01	0.01	0.01	0.01	0.01	0.01
Cr_2O_3	n.d.	n.d.	0.00	n.d.	0.02	0.03	n.d.	0.00	0.03	0.00	0.02
FeO	36.33	36.47	36.01	33.84	34.81	36.30	38.30	32.18	31.99	30.14	32.89
MnO	0.43	0.46	0.44	0.43	0.50	0.44	0.49	0.38	0.38	0.41	0.37
MgO	27.42	27.23	27.64	29.07	28.42	27.66	25.37	30.68	30.38	32.03	30.63
NiO	n.d.	n.d.	0.12	n.d.	0.09	0.07	n.d.	0.09	0.10	0.10	0.07
CaO	0.02	0.04	0.01	0.02	0.00	0.01	0.04	0.01	0.00	0.00	0.01
Total	99.33	99.59	100.06	98.19	100.08	100.51	98.61	99.99	99.36	99.54	100.51
Si *apfu*	0.990	0.995	0.999	0.983	1.003	0.999	0.989	1.002	1.003	1.002	0.997
Ti	0.000	0.000	0.000	0.000	0.000	0.000	0.000	0.000	0.000	0.000	0.000
Al	0.000	0.000	0.000	0.000	0.000	0.000	0.000	0.000	0.000	0.000	0.000
Cr			0.000		0.000	0.001		0.000	0.001	0.000	0.000
Fe	0.856	0.857	0.840	0.799	0.806	0.843	0.921	0.735	0.736	0.686	0.750
Mn	0.010	0.011	0.010	0.010	0.012	0.010	0.012	0.009	0.009	0.009	0.008
Mg	1.152	1.141	1.148	1.224	1.173	1.145	1.087	1.250	1.246	1.299	1.246
Ni			0.003		0.002	0.002		0.002	0.002	0.002	0.002
Ca	0.001	0.001	0.000	0.000	0.000	0.000	0.001	0.000	0.000	0.000	0.000
Total	3.010	3.005	3.001	3.017	2.997	3.000	3.011	2.998	2.997	2.998	3.003
Fa	0.426	0.431	0.422	0.395	0.408	0.424	0.456	0.375	0.372	0.346	0.376
Fo	0.574	0.569	0.578	0.605	0.593	0.576	0.544	0.625	0.628	0.654	0.624
#	4	4	10	4	10	15	4	10	15	15	15

These compositions represent the average results of # electron-microprobe analyses. Cation proportions are calculated on the basis of four atoms of oxygen per formula unit (*apfu*).

homogeneous, with compositions typically in the range $Hem_{3–6}$. However, in the few samples for which such titaniferous magnetite is scarce or absent, the ilmenite shows fine exsolution-induced lamellae of hematite, and the bulk composition is $Hem_{12–13}$. Ilmenite with 3–6 wt% Fe_2O_3 is far out of equilibrium with titaniferous magnetite and the coexisting ferromagnesian silicates for any reasonable range of total pressure and temperature. We conclude that the oxide in most Chugwater Anorthosite samples cooled along a magnetite isopleth (Frost *et al*. 1988, Fig. 4), which would have forced reduction of the ilmenite. It is significant that the rare ilmenite that has exsolved hematite and bulk compositions of $Hem_{12–13}$ occurs only in samples having a very high ilmenite:magnetite ratio and would therefore have cooled more nearly along an ilmenite isopleth. We infer that $Hem_{12–13}$ is close to the composition of all the Chugwater Anorthosite ilmenite prior to cooling. In our QUILF calculations, we took Hem_{13} as an upper limit on the ilmenite composition.

Sulfides. Pyrrhotite with lesser pentlandite and chalcopyrite occur as trace amounts in some samples of anorthosite, and are more abundant in some leucotroctolites and gabbroic anorthosites, especially those that occur at the ~4000 m level.

Low-temperature alteration. Some samples contain varying amounts of calcite, white mica, quartz, chlorite and epidote as products of low-temperature alteration in fractures and local pockets.

Petrographic evidence for magma mixing

Three main magma-types evidently contributed to the formation of the Chugwater Anorthosite: the parent to the anorthosites and gabbroic anorthosites, which apparently lacked olivine, and at least two variants of troctolitic or leucotroctolitic magma, both of which were magnesian relative to the anorthositic rocks. The troctolitic magmas associated with the lower portion of the stratigraphic Chugwater Anorthosite were relatively sodic, having normative An contents very similar to those of the anorthositic rocks, whereas those in the upper portion were distinctly more calcic (Fig. 8c). There is strong petrographic evidence for mixing of the troctolitic magmas with the gabbroic anorthosites.

The main petrographic evidence for mixing between the anorthositic magma and the associated leucotroctolitic magma or magmas is zoning in the minerals, especially plagioclase. In some cases, the zoning is obvious, as in the An2 and Gan3 units, where the

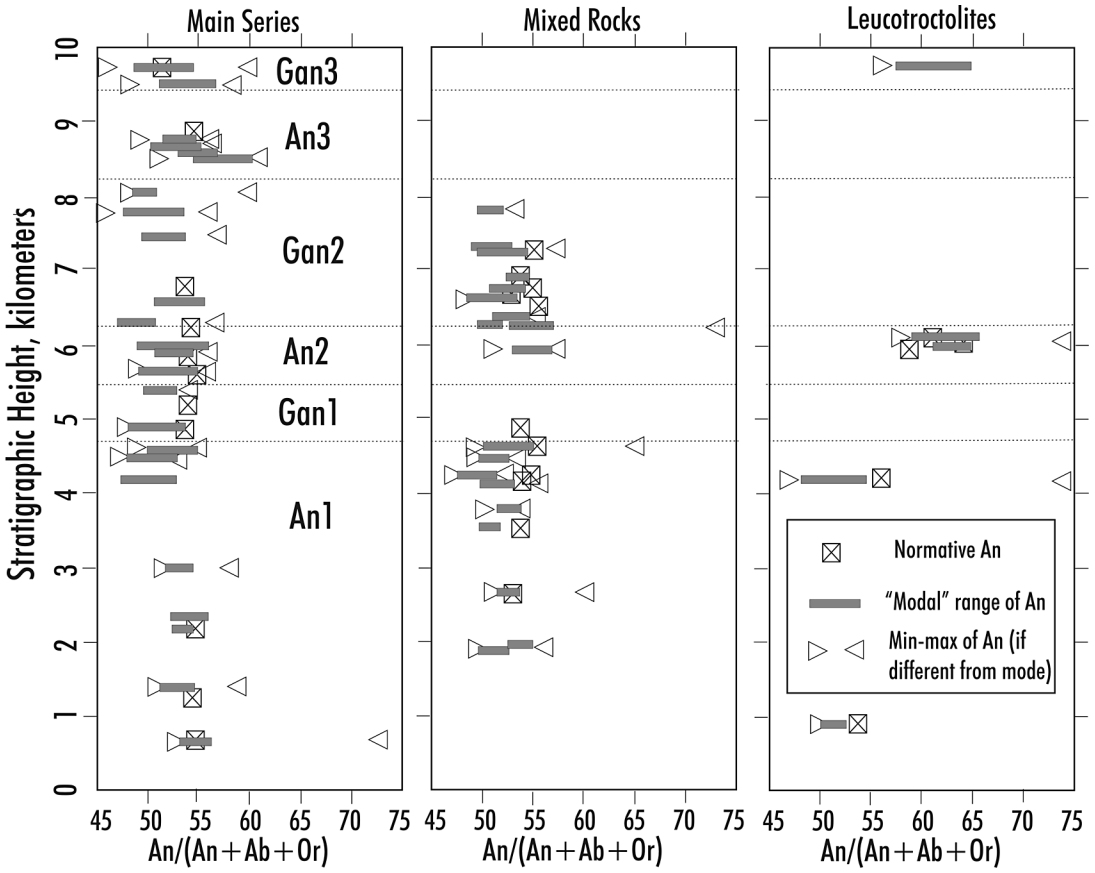

FIG. 7. Plagioclase compositions *versus* stratigraphic height in the Chugwater Anorthosite. The thick filled bar shows the range of most analyses, and the triangles show the extreme values found in each sample; boxes show normative An for analyzed samples, calculated from major-element compositions. a. Main-series Chugwater Anorthosite. b. Mixed rocks. c. Leucotroctolites.

invading leucotroctolite is An-rich, and plagioclase in the nearby gabbroic anorthosite shows strong reversed zoning. In other cases, where the plagioclase in the troctolite differs little from that of the anorthositic units, the zoning is much more subtle. Here the evidence for mixing stems largely from outermost zones of plagioclase megacrysts that are optically continuous with, but lack the oriented ilmenite lamellae of, the cores. Inclusion-free plagioclase in gabbroic anorthosite is especially prominent near olivine. In favorable cases, the zoning also shows up in one or more of the ferromagnesian minerals. Overall, these patterns of zoning suggest an abrupt change in the nature of the remaining liquid, consistent with magma mixing. Troctolites and leucotroctolites usually have sharp boundaries where they injected true anorthosite, presumably because the latter had little remaining liquid for mixing. In contrast, the contacts with gabbroic anorthosite are diffuse, suggesting that those layers still had sufficient residual liquid at the time of injection to allow significant mixing of magmas.

Importantly, when these *textural* criteria are applied to separate mixed from non-mixed samples, the latter (91 in total) are *all* found to be free of olivine, a phase that is distinctive of the troctolitic rocks. Of 51 anorthositic samples classified as mixed, in contrast, 40 contain olivine, and most of the rest are richer in Opx than non-mixed samples nearby, suggesting that any added olivine component may have reacted with SiO_2 to form additional Opx. The petrographic evidence for mixing is further supported by geochemical evidence (presented later). The Chugwater Anorthosite comprises all these units. For convenience, we refer to the anorthosites and gabbroic anorthosites that show no evidence of mixing as the "main series", and those that show such evidence as "mixed rocks".

An outcrop of gabbroic anorthosite near the northwestern end of An2 (BM 289, 5935 m level) contains abundant multiply-zoned crystals of iridescent plagioclase that show resorbed horizons, including the one that adorned the cover of the Journal of Petrology in 1998. This **z**oned **i**ridescent **p**lagioclase is so abundant in the vicinity of BM289 that we informally named the area "ZIP City" (Fig. 10). We interpret these crystals to be the result of repeated injections and mixing of hotter, more calcic leucotroctolitic magma into a gabbroic anorthosite layer of the Chugwater Anorthosite. Similar relationships occur in the Nain Plutonic Suite on Paul Island (Wiebe 1990, p. 9) and in the Port Manvers Run Intrusion (Michael Hamilton, written commun., 2009). A true anorthosite layer immediately above BM289 (An2), in contrast, contains pods of calcic troctolite and leucotroctolite at the 5960–6075 m level (samples KM36, 5960 m; BM52, 6000 m; BM269, 6075 m); here the contacts are sharp and distinct, with no evidence of mixing. These leucotroctolite inclusions are particularly interesting. We have mapped eight of them, ranging in size from approximately 3 to more than 10 meters across, over an along-strike distance of 8 km. Modal plagioclase decreases systematically from 89% in the northwest (BM52) to 71% in the southeast (KM36), whereas the An content decreases from 64 to 59%. Grain size also decreases from northwest to southeast. We consider it possible that these now-isolated inclusions were once part of a continuous intrusion that was broken apart during late-stage deformation of the enclosing Chugwater Anorthosite. If this interpretation is correct, then the feeder, which has not been not found, may have been near the region of BM52, where plagioclase phenocrysts accumulated by flow differentiation.

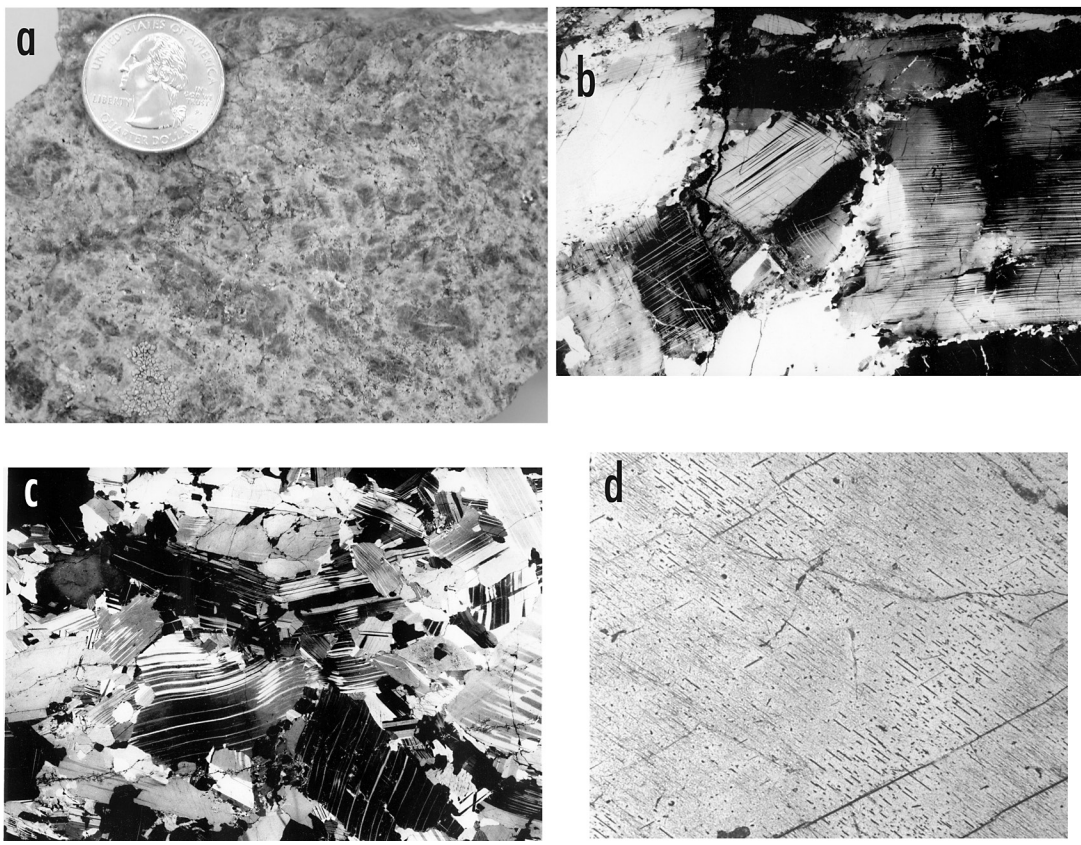

FIG. 8. Plagioclase textures in the Chugwater Anorthosite. a. Photograph of fragments of megacrysts (dark grey to black) in a matrix of neoblastic plagioclase (light grey). Coin is 2.4 cm across. b. Photograph of a thin section showing a portion of a megacryst with fine-grained neoblastic plagioclase surrounding it. Crossed polars; field of view 2.3 × 3.4 cm. c. Photograph of a thin section showing fragments of plastically deformed plagioclase megacrysts. Crossed polars; field of view 2.3 × 3.5 cm. d. Photomicrograph of a portion of a megacryst containing at least two orientations of ilmenite plates and rods. Note variation in size of the inclusions; smaller grains are more closely spaced, which is consistent with a constant volume-fraction of the inclusions. Width of field: 2.5 mm. Plane-polarized light.

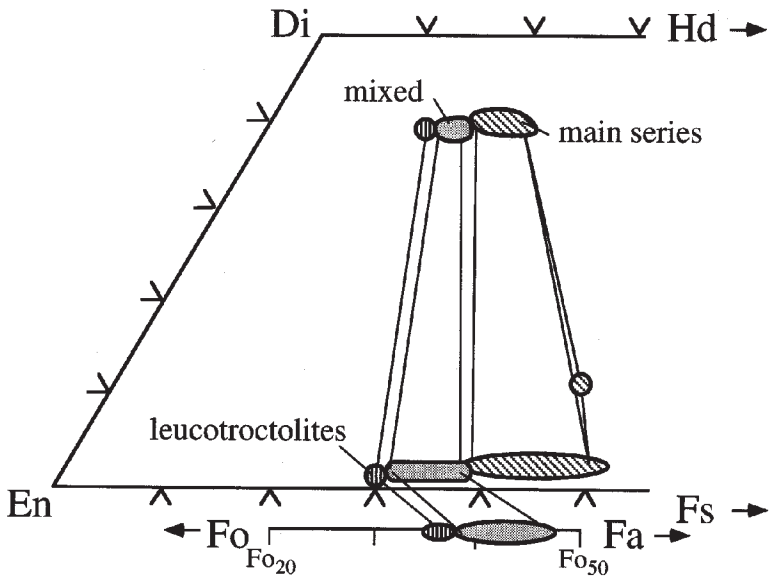

FIG. 9. Summary plot of pyroxene and olivine compositions, as projected through QUILF (Andersen *et al*. 1993).

The decrease in An content to the southeast may have resulted either from a decrease in the abundance of calcic phenocrysts or from a small admixture of residual liquid from the host anorthosite.

INTENSIVE PARAMETERS

Mineral compositions in plutonic rocks like the Chugwater Anorthosite typically undergo significant changes during cooling, both by exsolution and through exchange with other phases. In an attempt to "see through" these changes, we have applied QUILF equilibria (Lindsley & Frost 1992, Frost & Lindsley 1992, Andersen *et al*. 1993) to the Chugwater Anorthosite and summarize the results here.

Pressure

The Chugwater Anorthosite lacks a definitive geobarometer, so we estimate pressure from nearby rocks. Pressure for the northern margin of the Laramie Anorthosite Complex has been estimated to be near 3 kilobars (Sybille Pluton, Fuhrman *et al*. 1988; contact aureole, Grant & Frost 1990), whereas pressures for the southern margin are closer 3.5 to 4 kilobars (Maloin Ranch Pluton, Kolker & Lindsley 1989; contact aureole, Xirouchakis 1996). Because the Chugwater Anorthosite lies in the southern portion of the complex, we adopt an emplacement pressure of close to 3.5 kilobars. Clearly, however, if our reconstructed stratigraphy is correct, there must have been a range of several kbar from top to bottom of the Chugwater Anorthosite.

Temperature

The most robust thermometer in the Chugwater Anorthosite is the pigeonite thermometer, which is based on the X_{Fe} of the assemblage Opx + Cpx + Pig (Davidson & Lindsley 1989, Lindsley & Frost 1992, Fig. 2). Only a few samples show evidence for coexistence of all three pyroxenes, but for the remainder, the gap between pigeonite-bearing rocks (fictive $X_{Fe}^{Opx} = 0.53$) and pigeonite-absent rocks ($X_{Fe}^{Opx} = 0.49$) is small, and allows us to conclude that the upper portion of the Chugwater Anorthosite crystallized over a range of temperatures that included 1050°C.

Oxygen fugacity and silica activity

Because the compositions of the Fe–Ti oxides have been significantly reset on cooling, we use the QUIlF equilibria (Lindsley & Frost 1992) to calculate the oxygen fugacity and silica activity for the Chugwater Anorthosite. To facilitate comparison, we fix the temperature at 1050°C and the pressure at 3.5 kbar. For the $f(O_2)$ of olivine-bearing rocks, we use the location of the assemblage Ol–Opx–Cpx–Mgt–Ilm, which is dependent only on X_{Fe} of the silicates. For assemblages without olivine, we must calculate a range of possible oxygen fugacities, the lower limit being

that of olivine saturation, whereas the highest is that defined by ilmenite with $X_{hem} = 0.13$. We chose this value because it is close to the composition of ilmenite in Chugwater Anorthosite rocks that have cooled along an ilmenite isopleth (*i.e.*, those that originally had a very high ilmenite:magnetite ratio) (Frost *et al*. 1988, Fig. 4).

From these calculations, we determine that the main series crystallized at oxygen fugacities between FMQ and FMQ + 0.5, the leucotroctolites crystallized at oxygen fugacities around FMQ + 1.0, and the mixed rocks, at oxygen fugacities between FMQ and FMQ + 1.0. The calculated activity of silica (relative to quartz) of the main series varies from 0.7 at the base up to 1.0 at the top, where free quartz is locally found. In contrast, the silica activity of the mixed and troctolitic rocks lies in a restricted range, defined by olivine saturation, near 0.7 (Fig. 11).

Whole-Rock Chemistry

We selected 37 samples from the Chugwater Anorthosite for major-element analysis, together with a limited number of trace elements; for 32 of these, we also have more extensive information on the trace elements, including the REE (Tables 3a and 3b). These include 15 samples of the main series and 15 of mixed and troctolitic rocks from the stratigraphic Chugwater Anorthosite. Locations of analyzed samples are given in Figures 4, 5, and 6.

Sample preparation and analytical details

The weathering profile in anorthositic rocks of the LAC ranges from several centimeters to several meters in thickness. The majority of samples collected for this study were obtained using a water-cooled portable diamond drill, with core tubes 2.5 cm in diameter and

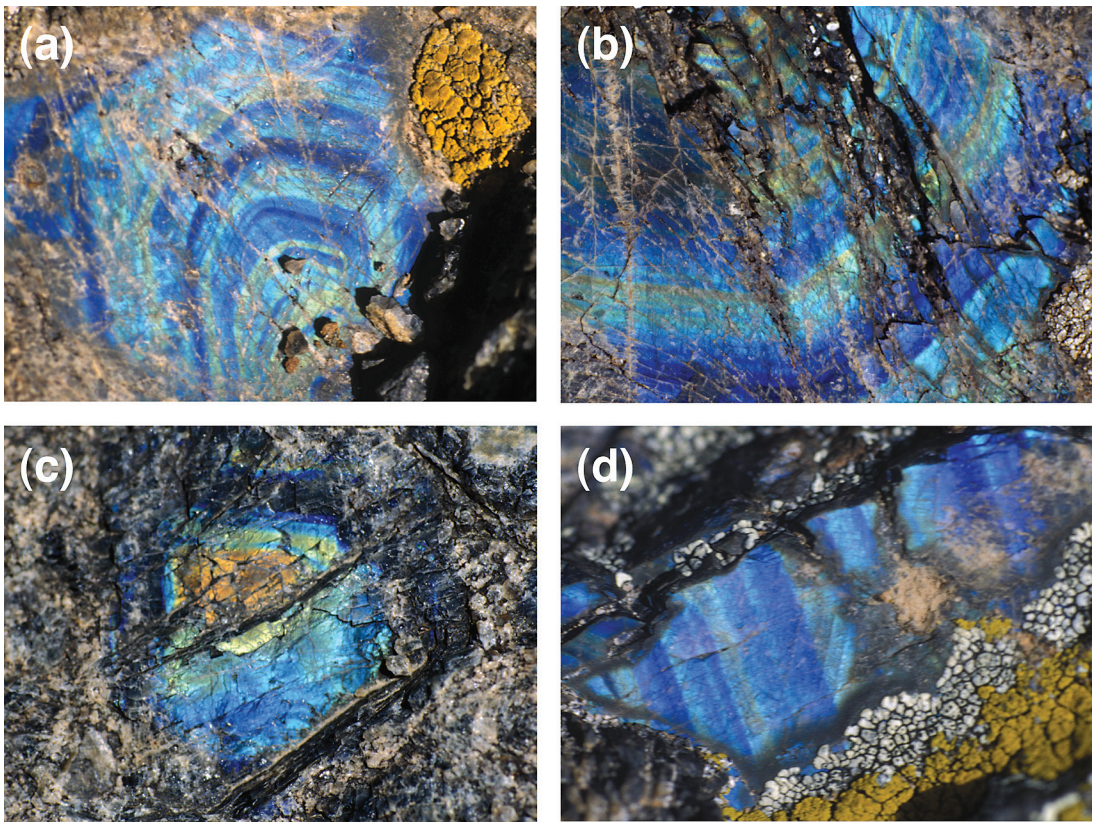

Fig. 10. Photographs of zoned iridescent plagioclase megacrysts (a, c, d approximately 3 cm across; b, approximately 4 cm across) from the Chugwater Anorthosite. Blue indicates $An_{52–53}$, green An_{53}, yellow An_{54}, orange An_{55}, all with approximately $Or_{3.5}$. Photos (a), (b), and (d) are from the BM289 locality, informally known as "ZIP City". The oscillatory zoning in (a), (b), and (d) is interpreted to result from repeated injections of leucotroctolitic magma, mixing with main-stage Chugwater magma (see text). Photo (c) shows mainly normal zoning, with only a small reversal evident.

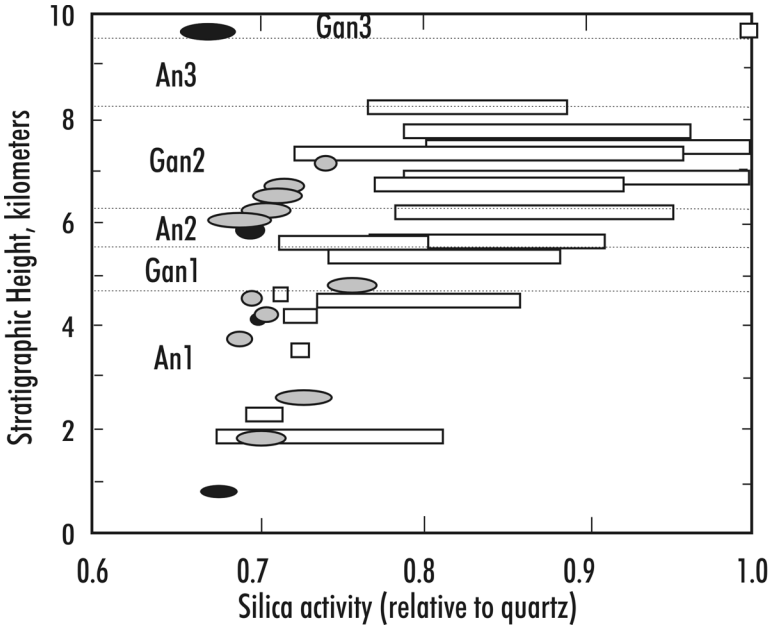

FIG. 11. Values of silica activity (relative to quartz) (Andersen *et al*. 1993), as a function of stratigraphic height. Rectangles: range of values for main-series (olivine-free) Chugwater Anorthosite. Upper limit of $a(SiO_2)$ is given by quartz saturation [$a(SiO_2) = 1$] or by assuming $X_{Hem} = 0.13$ in ilmenite (see text); the lower limit is that of olivine saturation. Grey ellipses: mixed rocks that contain olivine, black ellipses: leucotroctolites; for both of these, the range in calculated $a(SiO_2)$ is limited by the Fe/Mg values in the pyroxenes.

30 cm long. Depending on the grain size, we collected four to 10 cores for samples that were to be analyzed. The surface of each core was abraded with tungsten carbide (WC) paper to remove residue from the inside of the core tube. Coarse crushing was done in a Rocklabs hydraulic press between two flat WC plates (percussion method). A single aliquot (75 to 100 g) of homogenized coarsely crushed sample was powdered in a WC shatterbox for three minutes. All reported geochemical data in this study are from this aliquot.

Concentrations of the major elements were established by X-ray fluorescence spectrometry (XRAL Laboratories, Don Mills, Ontario) and by the ICP–MS method (Duke University, North Carolina).

Major elements

The major-element data hold few surprises, as compositions are dominated by the components of intermediate plagioclase. Normative mineralogy was calculated assuming that 15% of total Fe is ferric. Very low (cation) normative contents of *c* and *ne* for some samples probably are not real and may reflect uncertainties in the analyses. As expected, normative *ol* contents of most mixed and troctolitic rocks are distinctly higher than those reported for the main series, reaching 25% for troctolite BM273 (4180 m level). Figure 12 contains plots of normative *q* and *ol* as a function of stratigraphic level, with *ol* expressed as negative *q* for convenience. Most main-series rocks plot at or just above zero, whereas all mixed rocks and leucotroctolites show normative olivine. The modest contents of normative olivine for main-series rocks at 4900 to 6790 m mirrors the mainly lower values of X_{Fe}^{Opx} (Fig. 13) and higher *mg#* in that interval.

Whole-rock *mg* numbers (Table 1) do not vary systematically with stratigraphic height. In anorthositic rocks, *mg* numbers are problematical, as they are extremely sensitive to the relative proportions of ferromagnesian silicate and Fe–Ti oxide crystals that were present at the stage when the residual liquid was expelled, as well as to errors in chemical analysis resulting from very low abundances of Mg and Fe. In samples classified as of the main series (non-mixed) on petrographic criteria, *mg#* ranges from 0.41 to 0.57. For mixed rocks, *Mg#* ranges mainly between 0.57 and 0.62, with the values dropping to 0.53 (7256 m level) and 0.49 (7585 m level). This drop is closely reflected

TABLE 3a. MAJOR-ELEMENT COMPOSITIONS OF SAMPLES FROM THE CHUGWATER ANORTHOSITE

	Main series and mixed rocks														
Sample	BM 137	BM 146	BM 136,142	BM 187	BM 188	BM 238	BM 241	KM 065	KM 006	KM 233	KM 044	KM 046	KM 049	BM 053	KM 012
height, m	688	1243	1404	2180	2680	3005	3550	4180	4250	4630	4900	4900	5200	5600	5850
Unit	An1	An1	An1	An1	An1 Mix	An1	An1 Mix	An1 Mix	An1 Mix	An1 Mix	Gan1	Gan1	Gan1	Gan1	An2
SiO_2 wt%	54.40	53.20	53.00	53.70	51.12	52.50	52.40	51.60	52.00	52.00	52.00	52.00	51.60	52.80	53.50
TiO_2	0.13	0.37	0.35	0.11	0.51	0.11	0.44	0.40	0.26	0.26	0.26	0.32	0.31	0.39	0.37
Al_2O_3	27.40	26.80	26.90	29.00	24.64	28.70	24.20	26.10	23.90	25.20	26.30	27.00	25.90	26.30	25.85
Fe_2O_3 (tot)	0.84	1.95	1.98	0.69	4.86	0.79	4.95	2.80	5.19	3.38	2.56	1.93	2.63	3.00	2.93
Fe_2O_3	0.13	0.29	0.30	0.10	0.73	0.12	0.74	0.42	0.78	0.51	0.38	0.29	0.39	0.45	0.44
FeO	0.64	1.49	1.51	0.53	3.72	0.60	3.79	2.14	3.97	2.58	1.96	1.48	2.01	2.29	2.24
MnO	0.02	0.03	0.03	0.01	0.05	0.01	0.07	0.03	0.07	0.05	0.03	0.02	0.03	0.03	0.05
MgO	0.32	0.63	0.77	0.22	2.99	0.25	2.86	1.70	3.68	2.12	1.41	0.81	1.48	1.40	1.45
CaO	11.40	11.10	10.90	10.90	9.97	11.20	9.96	10.10	9.78	10.40	10.10	10.30	10.00	10.40	10.60
Na_2O	4.52	4.42	4.38	4.60	4.24	4.30	4.04	4.34	3.89	4.07	4.31	4.42	4.20	4.21	4.24
K_2O	0.52	0.58	0.74	0.55	0.65	0.44	0.62	0.62	0.56	0.57	0.69	0.69	0.67	0.62	0.66
P_2O_5	0.02	0.03	0.10	0.02	0.08	0.02	0.06	0.06	0.03	0.06	0.07	0.05	0.05	0.08	0.06
LOI	0.50	0.50	0.25	0.40	0.24	0.95	0.35	0.60	0.30	1.90	0.85	1.15	1.65	1.00	0.33
Total	100.09	99.63	99.40	100.20	99.13	99.27	99.96	98.34	99.68	100.03	98.56	98.72	98.52	100.23	100.05
mg# cat	0.47	0.43	0.48	0.43	0.59	0.43	0.57	0.59	0.62	0.59	0.56	0.49	0.57	0.52	0.54
Norm An	0.55	0.54	0.54	0.55	0.53	0.57	0.54	0.54	0.55	0.55	0.54	0.54	0.54	0.55	0.54
q	1.50	0.45	0	0.80	0	1.02	0	0	0	0	0	0	0	0.30	0.66
or	3.03	3.40	4.34	3.19	3.79	2.59	3.64	3.68	3.29	3.38	4.10	4.10	4.02	3.64	3.86
ab	39.98	39.41	39.02	40.49	37.22	38.49	36.04	39.18	34.73	36.71	38.92	39.94	38.30	37.57	37.66
an	52.16	51.22	51.15	52.89	46.07	55.27	45.78	50.05	45.84	49.04	50.07	50.90	50.05	50.73	49.03
c	0	0	0	0	0	0.91	0	0.05	0	0	0.24	0.49	0.23	0	0
ne	0	0	0	0	0.39	0	0	0	0	0	0	0	0	0	0
Di	2.64	2.52	1.48	0	1.97	0	2.3	0	1.67	1.82	0	0	0	0.03	2.04
Wo	1.32	1.26	0.74	0	0.98	0	1.15	0	0.83	0.91	0	0	0	0.02	1.02
En	0.71	0.65	0.41	0	0.63	0	0.71	0	0.55	0.58	0	0	0	0.01	0.61
Fs	0.61	0.61	0.33	0	0.35	0	0.44	0	0.29	0.33	0	0	0	0.01	0.41
Hy	0.3	2.09	2.89	1.19	0	1.4	8.3	2	9.03	6.85	4.02	2.79	5.85	6.55	5.64
En	0.16	1.09	1.61	0.6	0	0.69	5.15	1.3	5.91	4.35	2.47	1.59	3.66	3.83	3.35
Fs	0.14	1.01	1.28	0.59	0	0.71	3.16	0.7	3.12	2.5	1.55	1.2	2.19	2.72	2.29
Ol	0	0	0.12	0	8.87	0	2.41	3.94	4.17	1.12	1.77	0.86	0.58	0	0
Fo	0	0	0.07	0	5.69	0	1.49	2.56	2.73	0.71	1.09	0.49	0.36	0	0
Fa	0	0	0.05	0	3.19	0	0.92	1.37	1.44	0.41	0.68	0.37	0.22	0	0
Mt	0.13	0.3	0.31	0.11	0.76	0.12	0.77	0.44	0.81	0.53	0.4	0.31	0.42	0.47	0.45
Ilm	0.18	0.51	0.48	0.15	0.71	0.15	0.61	0.56	0.36	0.36	0.37	0.45	0.44	0.54	0.51
Ap	0.08	0.1	0.21	0.04	0.22	0.04	0.15	0.11	0.1	0.17	0.11	0.17	0.11	0.17	0.14
Fsp	95.2	94	94.5	96.6	87.1	96.4	85.46	92.9	83.9	89.1	93.1	94.9	92.4	91.9	90.6
Source:	X,M	X,M	X	X,M	M	X,M	X,M	X,M	X,M	X,M	X,M	X,M	X,M	X,M	X,M

Notes: X: Major elements and limited minor elements by XRF from XRAL. M: Minor and trace elements and major elements for BM188 and KM033 by ICP–MS by William P. Meurer (Duke University). Height is given above an arbitrary base.

by X_{Fe}^{Opx} in the mixed rocks (Fig. 13). The higher *mg* values for the mixed rocks almost certainly reflect the admixture of Mg-rich leucotroctolite material, which has *mg#* ranging from 0.63 to 0.69. Samples KM44 and KM46 (4900 m level) were collected less than 1 m apart, yet their *mg#* are 0.49 and 0.56. The distribution of *mg#* approximately reflects that of X_{Fe}^{Opx} (0.39–0.41 in KM44; 0.35–0.38 in KM46). We suspect that the higher mg# of KM46, as well as its range of X_{Fe}^{Opx}, may reflect some mixing of leucotroctolite into this sample.

Cation norms for the rocks of the main series are plagioclase-rich (as expected): normative feldspar totals from 80.1 to 95.6%. The normative content of Or is quite close to the measured Or contents of Chugwater Anorthosite plagioclase, consistent with the fact that no separate K-feldspar phase is seen. Thus it is appropriate

TABLE 3a (cont'd). MAJOR-ELEMENT COMPOSITIONS OF SAMPLES FROM THE CHUGWATER ANORTHOSITE

	Main series and mixed rocks										Troctolite and Leucotroctolites				
Sample	BM 281	KM 094	KM 069	KM 087	KM 092	KM 091	KM 086	KM 033	KM 013	KM 020	BM 160	BM 273	KM 036	BM 052	BM 269
height, m	6245	6525	6615	6715	6785	6790	6895	7256	8860	9740	863	4180	5960	6000	6075
Unit	Gan2	Gan2 Mix	Gan2 Mix	Gan2 Mix	Gan2 Mix	Gan2	Gan2 Mix	Gan2 Mix	An3	Gan3	An1 Lt	An1 Troct	An2 Lt	An2 Lt	An2 Lt
SiO_2 wt%	50.80	50.50	49.70	51.60	49.80	51.40	51.90	50.44	52.30	53.00	49.60	46.90	46.90	49.70	48.10
TIO_2	0.28	0.37	0.31	0.62	0.35	0.51	0.42	0.68	0.43	0.46	1.03	0.20	0.47	0.18	0.31
Al_2O_3	24.10	24.90	23.80	25.60	24.50	25.40	23.60	24.71	25.90	22.00	19.90	18.50	20.20	26.70	24.10
Fe_2O_3 (tot)	5.25	4.54	5.44	3.41	4.47	3.74	5.11	5.74	2.25	5.77	9.42	12.00	8.97	3.57	5.78
Fe_2O_3	0.79	0.68	0.82	0.51	0.67	0.56	0.77	0.12	0.34	0.87	1.41	1.80	1.35	0.54	0.87
FeO	4.01	3.47	4.16	2.61	3.42	2.86	3.91	2.19	1.72	4.41	7.20	9.18	6.86	2.73	4.42
MnO	0.05	0.05	0.06	0.03	0.05	0.04	0.08	0.06	0.05	0.11	0.12	0.13	0.10	0.04	0.07
MgO	3.15	2.60	3.70	1.22	2.62	1.63	2.79	2.81	0.68	2.87	7.08	10.60	8.59	2.98	4.27
CaO	9.25	9.78	9.47	10.20	9.77	10.10	9.62	10.42	10.90	9.53	8.47	7.15	8.71	11.60	10.40
Na_2O	3.81	3.90	3.77	4.35	3.93	4.23	3.87	4.03	4.11	3.75	3.27	2.81	2.90	3.38	3.21
K_2O	0.68	0.65	0.58	0.72	0.64	0.70	0.66	0.69	0.79	0.79	0.49	0.40	0.44	0.31	0.48
P_2O_5	0.02	0.10	0.06	0.08	0.09	0.13	0.12	0.11	0.16	0.36	0.22	0.05	0.04	0.03	0.03
LOI	2.45	2.00	1.90	1.00	2.80	0.95	0.02	0.46	1.30	1.00	0.45	0.05	1.05	1.55	2.05
Total	99.87	99.36	98.79	98.82	99.00	98.70	98.18	99.76	98.87	99.66	100.05	98.78	98.37	100.03	98.80
mg# cat	0.58	0.57	0.61	0.45	0.58	0.50	0.56	0.53	0.41	0.54	0.64	0.67	0.69	0.66	0.63
Norm An	0.54	0.55	0.55	0.53	0.55	0.53	0.54	0.55	0.55	0.52	0.54	0.56	0.59	0.64	0.61
q	0	0	0	0	0	0	0.08	0	1.03	2.13	0	0	0	0	0
or	4.08	3.90	3.49	4.29	3.88	4.18	3.94	4.06	4.72	4.72	2.90	2.37	2.64	1.83	2.90
ab	34.74	35.54	34.51	39.42	36.21	38.35	35.11	34.36	37.35	34.04	29.41	25.35	26.46	30.38	29.49
an	46.28	48.78	47.22	48.65	48.57	48.73	45.55	47.01	50.49	41.32	38.24	35.38	41.47	56.83	51.10
c	0.44	0.18	0	0	0	0	0	0	0	0	0	0.59	0	0	0
ne	0	0	0	0	0	0	0	0.96	0	0	0	0	0	0	0
Di	0	0	0.23	1.57	0.57	1.5	1.56	2.66	2.54	3.18	1.93	0	1.75	0.52	1.2
Wo	0	0	0.12	0.79	0.28	0.75	0.78	1.33	1.27	1.59	0.96	0	0.87	0.26	0.6
En	0	0	0.07	0.42	0.18	0.43	0.47	0.79	0.63	0.92	0.66	0	0.63	0.18	0.4
Fs	0	0	0.04	0.36	0.11	0.32	0.31	0.54	0.64	0.67	0.3	0	0.24	0.08	0.2
Hy	9.65	5.36	4.55	1.53	2.59	2.04	12.12		2.56	12.25	13.92	9.07	4.30	3.38	2.90
En	5.97	3.31	2.95	0.83	1.61	1.17	7.31		1.27	7.09	9.56	6.30	3.10	2.34	1.93
Fs	3.67	2.06	1.6	0.7	0.98	0.88	4.8		1.29	5.16	4.36	2.77	1.2	1.04	0.97
Ol	3.47	4.84	8.55	2.98	6.82	3.88	0	8.78	0	0	10.23	24.97	21.21	6.21	10.97
Fo	2.15	2.98	5.54	1.61	4.23	2.21	0	5.19	0	0	7.02	17.33	15.28	4.29	7.3
Fa	1.32	1.86	3.01	1.37	2.59	1.67	0	3.58	0	0	3.2	7.63	5.93	1.92	3.67
Mt	0.84	0.72	0.87	0.54	0.72	0.59	0.81	0.89	0.36	0.91	1.48	1.89	1.43	0.56	0.93
Ilm	0.4	0.52	0.44	0.87	0.49	0.72	0.6	0.94	0.61	0.65	1.44	0.29	0.66	0.25	0.44
Ap	0.11	0.15	0.13	0.15	0.15	0	0.23	0.34	0.34	0.8	0.46	0.08	0.09	0.04	0.06
Fsp	85.1	88.2	85.2	92.4	88.7	91.3	84.6	85.4	92.6	80.1	70.6	63.1	70.6	89	83.5
Source	X,M	X,M	X	X,M	X,M	X,M	X,M	M	X,M	X,M	X,M	X,M	X,M	X,M	X,M

Notes: X: Major elements and limited minor elements by XRF from XRAL. M: Minor and trace elements and major elements for BM188 and KM033 by ICP–MS by William P. Meurer (Duke University). Height is given above an arbitrary base.

to use total normative feldspar as an estimate for the amount of modal plagioclase. Normative An contents [an/(an + ab + or)] tend to lie at the upper end or even above the range of the most abundant *modal* feldspar compositions measured by electron microprobe (Figs. 7a, b, c). There are probably several explanations for this phenomenon. First, because of the geometric relationship between the volume of a solid and the surface exposed by a random section through it, the most calcic portion of a normally zoned plagioclase may not be exposed at the thin-section surface, or if exposed, may not have been analyzed. Second, the norm calculation ignores the small but real Ca-Tschermaks component of the pyroxenes, which is slightly dominant over their Jd component. Third, xenocrysts of calcic plagioclase may be underrepresented in the population of plagioclase

TABLE 3b. MINOR- AND TRACE-ELEMENT DATA ON SAMPLES FROM THE CHUGWATER ANORTHOSITE

	Main series and mixed rocks														
#	BM137	BM146	BM136*	BM187	BM188	BM238	BM241	KM065	KM006	BM233	KM044	KM046	KM049	BM053	KM012
m	688	1243	1404	2180	2680	3005	3550	4180	4250	4630	4900	4900	5200	5600	5850
Unit	An1	An1	An1	An1	An1 Mix	An1	An1 Mix	An1 Mix	An1 Mix	An1 Mix	Gan1	Gan1	Gan1	Gan1	An2
Li	6.79	6.17		6.74	4.55	5.19	4.88	4.69	4.05	3.58	5.03	5.45	5.09	3.41	4.93
Sc	1.64	1.63		0.55	2.90	2.53	5.19	3.04	2.62	2.02	3.30	2.00	3.97	6.23	4.05
V	3.5	24.0	27.0	4.1	37.3	3.5	48.8	24.0	24.8	17.7	20.9	12.3	27.5	37.5	36.5
Cr	2.98	13.19		4.38	55.1	2.21	31.31	17.09	24.16	2.33	7.94	3.02	22.5	19.8	17.7
Co	25.0	17.6	22.0	18.8	45.4	19.4	33.6	44.6	39.7	27.7	52.7	32.2	37.6	29.5	21.1
Ni	4.1	11.4		4.1	62.9	3.8	74.0	33.9	74.9	38.0	15.4	13.0	15.7	15.5	13.0
Cu	1.54	3.81		1.64	4.99	0.87	11.94	4.59	4.22	9.33	2.65	3.69	4.72	4.61	3.49
Zn	13.0	13.3	b.d.l.	20.0	38.9	14.5	38.2	43.2	37.7	49.8	34.2	22.2	28.2	46.1	27.8
Ga	30.9	33.2	21.0	28.6	34.4	23.8	33.6	33.2	25.5	33.1	28.4	31.1	33.0	30.7	32.8
Rb	2.09	2.80	3.12	3.09	4.32	2.43	4.08	3.81	3.31	2.95	5.55	5.07	4.41	4.26	4.42
Sr	949	921	833	963	849	903	852	897	836	864	900	912	879	911	901
Y	1.18	1.76	2.70	0.82	3.85	0.54	3.51	3.18	1.72	2.52	3.26	3.33	2.95	3.84	3.16
Zr	3.1	9.4	21.0	2.1	18.8	2.5	23.3	20.4	9.7	13.8	16.6	19.0	18.8	19.9	29.8
Nb	0.21	0.99	2.60	0.08	2.59	0.10	1.55	2.21	0.79	1.32	1.07	2.07	1.63	1.51	1.37
Mo	0.195	0.259		0.177	0.313	0.207	0.300	0.305	0.222	0.360	0.315	0.316	0.306	0.275	0.273
Cd	0.013	0.012		0.012	0.018	0.006	0.039	0.025	0.016	0.014	0.020	0.014	0.013	0.028	0.021
Cs	0.029	0.018		0.099	0.042	0.074	0.031	0.042	0.023	0.037	0.109	0.090	0.038	0.032	0.033
Ba	327	362	220	369	386	298	387	387	342	382	398	411	393	413	400
Hf	0.075	0.257	0.500	0.039	0.510	0.051	0.529	0.529	0.255	0.362	0.409	0.450	0.478	0.495	0.623
Ta	0.128	0.126	0.160	0.077	0.232	0.082	0.134	0.247	0.103	0.117	0.224	0.237	0.196	0.168	0.146
Tl	0.147	0.176		0.219	0.368	0.264	0.384	0.329	0.219	0.245	0.531	0.457	0.306	0.327	0.287
Pb	1.08	1.07	b.d.l.	1.89	1.41	0.98	1.92	1.50	1.31	1.47	1.96	1.85	1.55	1.82	1.69
Th	0.044	0.098	0.120	0.027	0.288	0.029	0.197	0.175	0.105	0.287	0.332	0.361	0.355	0.279	0.231
U	0.055	0.034	0.050	0.018	0.098	0.007	0.080	0.065	0.040	0.092	0.118	0.142	0.132	0.079	0.088
La	3.00	4.07	4.70	3.03	5.75	2.58	5.07	4.95	3.83	5.21	6.00	6.35	5.52	5.78	5.85
Ce	4.98	7.25	9.16	4.99	11.40	4.36	9.56	9.39	7.14	9.88	11.4	12.2	10.6	11.1	11.1
Pr	0.602	0.889	0.950	0.576	1.42	0.51	1.13	1.19	0.85	1.22	1.38	1.49	1.28	1.41	1.36
Nd	2.11	3.41	4.20	2.06	5.76	1.89	4.48	4.50	3.26	4.67	5.42	5.99	4.94	5.64	5.33
Sm	0.323	0.596	0.870	0.298	1.059	0.257	0.867	0.789	0.544	0.836	0.956	1.07	0.829	1.09	0.984
Eu	0.99	1.09	1.10	1.05	1.17	0.91	1.18	1.15	1.08	1.07	1.23	1.23	1.15	1.19	1.23
Gd	0.268	0.512	0.730	0.215	0.951	0.193	0.782	0.810	0.483	0.748	0.836	0.940	0.758	0.992	0.898
Tb	0.040	0.072	0.110	0.032	0.140	0.026	0.123	0.122	0.070	0.105	0.121	0.131	0.114	0.136	0.134
Dy	0.172	0.342	0.540	0.146	0.674	0.124	0.635	0.628	0.367	0.475	0.687	0.659	0.582	0.741	0.702
Ho	0.032	0.068	0.090	0.025	0.134	0.015	0.116	0.113	0.068	0.086	0.125	0.120	0.110	0.138	0.131
Er	0.089	0.174	0.250	0.053	0.334	0.039	0.329	0.310	0.173	0.243	0.332	0.307	0.307	0.369	0.355
Yb	0.063	0.147	0.190	0.037	0.289	0.026	0.285	0.282	0.160	0.211	0.297	0.244	0.268	0.308	0.320
Lu	0.010	0.023	0.027	0.005	0.043	0.004	0.043	0.038	0.024	0.028	0.045	0.041	0.040	0.049	0.052
	X,M	X,M	A	X,M	M	X,M	X,M	X,M	X,M	X,M	X,M	X,M	X,M	X,M	X,M

Notes: Concentrations are expressed in ppm. Source: X: Major elements and limited minor elements by XRF from XRAL. M: Minor and trace elements by ICP–MS by William P. Meurer (Duke University). A: Minor and trace elements by ICP–MS (Actlabs). Units (An1, An2, Gan2, *etc.*) indicate the dominant lithology (Anorthosite, >90% Pl; Gabbroic anorthosite, 80–90% Pl) shown in Figures 2, 4, and 5. "Mix" means mixed Chugwater Anorthosite and leucotroctolite. b.d.l.: below detection limit. * BM136 and BM142; m: height in meters above an arbitrary base.

analyzed by microprobe. Finally, the XRF analyses of the whole rocks may have slightly underestimated their Na_2O contents.

Trace elements

For most analyzed samples, we have data for 21 trace elements plus the rare-earth elements; analytical details for the ICP–MS method are given in Meurer *et al.* (1999, p. 147-148). As one might expect, Sr is highly correlated with total feldspar in each rock. Elements such as Rb, V, Y, Sc, Hf, Nb, Ta, Tl, Th and U, which are largely incompatible in plagioclase, show considerable variation. All increase by factors of 3 to 10 from bottom to top of the Chugwater Anorthosite (Fig. 14). The increase is far from smooth; it is punctuated by

TABLE 3b (cont'd). MINOR- AND TRACE-ELEMENT DATA ON SAMPLES FROM THE CHUGWATER ANORTHOSITE

	Main series and mixed rocks										Troctolite and Leucotroctolites				
#	BM281	KM094	KM069	KM087	KM092	KM091	KM086	KM033	KM013	KM020	BM160	BM273	KM036	BM052	BM269
m	6245	6525	6615	6715	6785	6790	6895	7256	8860	9740	863	4180	5960	6000	6075
Unit	Gan2	Gan2 Mix	Gan2 Mix	Gan2 Mix	Gan2 Mix	Gan2	Gan2 Mix	Gan2 Mix	An3	Gan3	An1 Lt	An1 Tr	An2 Lt	An2 Lt	An2 Lt
Li	8.01	4.56		4.51	4.10	2.96	6.04	7.82	8.10	7.64	5.28	5.68	2.98	5.05	2.64
Sc	3.36	3.79		7.06	3.11	7.20	9.42	5.63	3.90	11.06	6.47	3.39	6.43	5.05	5.52
V	33.4	24.3		71.6	21.5	39.9	40.1	62.9	25.0	39.3	54.7	25.5	32.8	24.6	31.0
Cr	3.52	4.09		40.7	7.1	12.5	19.4	7.53	1.87	39.13	97.8	64.8	54.2	50.8	47.8
Co	34.1	33.1		33.5	47.2	33.0	41.3	58.9	16.0	29.2	62.7	101.1	87.8	32.4	43.2
Ni	69.0	40.8		21.0	50.3	22.4	15.1	49.0	18.1	12.1	156	257	229	44.9	86.0
Cu	7.66	3.89		8.41	6.62	7.72	5.75	11.30	5.98	5.40	9.20	10.6	15.8	18.2	21.9
Zn	34.9	39.4		53.2	35.0	32.1	48.0	58.1	26.2	54.4	62.8	84.4	67.5	23.4	45.4
Ga	27.1	30.0		33.3	27.8	36.1	28.7	28.0	27.2	30.9	25.1	22.1	23.6	24.0	22.1
Rb	4.54	6.10	2.00	5.68	6.01	6.19	5.54	6.20	7.64	11.09	3.66	2.11	2.17	1.88	2.05
Sr	732	801	718	808	769	844	785	780	842	715	674	634	601	759	637
Y	3.09	4.15	5.00	4.83	4.12	6.55	7.41	7.09	6.83	14.77	6.50	1.40	2.82	1.56	2.18
Zr	20.4	24.9	33.0	29.9	34.9	33.4	34.4	41.7	21.1	33.9	20.8	7.24	13.1	4.30	7.74
Nb	1.41	2.73	2.00	3.24	2.81	3.12	2.33	3.61	4.15	4.48	4.76	0.421	1.06	0.150	0.599
Mo		0.167		0.319	0.410	0.420	0.395	0.359	0.461	0.425	0.349	0.226	0.365	0.200	0.187
Cd	0.005	0.019		0.028	1.19	0.031	0.039	1.93		0.049	0.057	0.024	0.026	0.042	0.024
Cs	0.061	0.124		0.068	0.129	0.093	0.063	0.091	0.088	0.211	0.054	0.038	0.010	0.008	0.031
Ba	395	374	336	392	348	415	386	402	427	430	299	260	267	204	260
Hf	0.495	0.689		0.777	0.864	0.852	0.804	1.10	0.590	0.896	0.565	0.157	0.360	0.145	0.227
Ta	0.141	0.214		0.277	0.252	0.244	0.230	0.349	0.303	0.316	0.332	0.110	0.229	0.065	0.091
Tl	0.164	0.602		0.435	0.515	0.418	0.472	0.559	0.620	1.051	0.217	0.131	0.120	0.091	0.165
Pb	2.14	1.90		1.83	1.77	1.89	2.01	2.06	2.51	3.62	1.26	1.09	3.65	0.86	1.65
Th	0.396	0.223		0.441	0.577	0.405	0.349	0.464	0.995	1.455	0.238	0.079	0.075	0.026	0.066
U	0.091	0.077		0.146	0.204	0.129	0.127	0.153	0.213	0.401	0.091	0.030	0.025	0.006	0.019
La	5.63	7.23		6.82	6.84	8.04	7.51	8.50	10.66	15.95	6.72	2.76	4.33	2.28	3.09
Ce	10.9	13.8		13.4	13.7	16.2	15.3	17.8	21.6	35.2	14.4	5.09	8.22	4.42	5.78
Pr	1.31	1.70		1.64	1.70	2.06	1.97	2.29	2.74	4.56	1.94	0.60	1.01	0.57	0.71
Nd	5.09	6.88		6.91	6.70	8.72	8.17	9.68	11.2	19.6	8.28	2.35	3.87	2.30	2.89
Sm	0.94	1.32		1.26	1.21	1.75	1.70	1.94	2.12	3.87	1.65	0.376	0.751	0.444	0.561
Eu	1.05	1.15		1.26	1.10	1.28	1.21	1.20	1.29	1.67	1.01	0.770	0.983	0.682	0.840
Gd	0.787	1.165		1.19	1.12	1.58	1.63	1.81	1.78	3.66	1.69	0.327	0.750	0.385	0.537
Tb	0.114	0.164		0.176	0.166	0.238	0.241	0.263	0.257	0.521	0.235	0.049	0.114	0.050	0.080
Dy	0.580	0.868		0.974	0.867	1.23	1.39	1.43	1.39	2.78	1.26	0.280	0.581	0.300	0.445
Ho	0.114	0.170		0.189	0.161	0.247	0.269	0.267	0.255	0.540	0.234	0.045	0.107	0.052	0.082
Er	0.293	0.432		0.472	0.425	0.616	0.739	0.693	0.646	1.376	0.620	0.124	0.304	0.129	0.212
Yb	0.268	0.361		0.417	0.371	0.540	0.692	0.571	0.529	1.132	0.524	0.129	0.278	0.116	0.172
Lu	0.040	0.056		0.061	0.057	0.078	0.108	0.087	0.077	0.175	0.073	0.024	0.045	0.016	0.027
	X,M	X,M	X	X,M	X,M	X,M	X,M	M	X,M	X,M	X,M	X,M	X,M	X,M	X,M

Notes: Concentrations are expressed in ppm. Source: X: Major elements and limited minor elements by XRF from XRAL. M: Minor and trace elements by ICP–MS by William P. Meurer (Duke University). Units (An1, An2, Gan2, *etc.*) indicate the dominant lithology (Anorthosite, >90% Pl; Gabbroic anorthosite, 80–90% Pl) shown in Figures 2, 4, and 5. "Mix" means mixed Chugwater Anorthosite and leucotroctolite. m: height in meters above anarbitrary base.

excursions that approximately mirror the variations in X_{Fe}^{Opx}. In Unit 1 (0–5590 m), the average increase is by a factor of approximately two. In Unit 2 (5590–8300 m), the increase is also by the same factor, but the rate of increase is greater because of the smaller stratigraphic interval. We have only two analyzed samples in Unit 3 (8300 – 10000 m), but trace-element concentrations also increase upward between the two. Zinc, Cu, and Ni are strongly enriched in the leucotroctolites relative to the anorthositic rocks. Those elements are also slightly enriched in the mixed rocks relative to the main-series Chugwater Anorthosite.

The rare-earth elements

The chondrite-normalized REE patterns in the main-series Chugwater Anorthosite have positive Eu anomalies (Eu/Eu*) that range from >10 to just slightly

greater than one (Fig. 15a). The value of Eu/Eu* and the slope of the patterns decrease with overall abundance; both features also mainly decrease with increasing stratigraphic height, but there are excursions that approximately mirror the variations in other incompatible trace elements (*e.g.*, Fig. 14). Of particular interest is the near-absence of a europium anomaly at the top of the Chugwater Anorthosite; under the reasonable assumption that the plagioclase megacrysts here retain a positive Eu anomaly, then the remainder of the sample must have a corresponding negative anomaly. The REE patterns for the medium-An leucotroctolites are similar to those of the main-series Chugwater Anorthosite (but with less variation in abundance) (Fig. 15b).

Discussion

Significance of Fe–Ti oxide inclusions in plagioclase megacrysts

We believe that the Fe–Ti oxide inclusions in plagioclase place important constraints on the evolution of the Chugwater Anorthosite; it is thus necessary to understand their origin. We consider three possible origins: (1) entrapment of early Fe–Ti oxide by growing plagioclase, (2) late-stage deposition by circulating fluids, and (3) exsolution from the plagioclase. We reject case (1) on four very different grounds. First, it is most implausible that the parental liquid would have become saturated with Fe–Ti oxide *before* plagioclase, and the preferred orientation of the inclusions is also hard to explain if they had simply been engulfed by growing plagioclase. Second, favorable sections show that different sets of albite-twin lamellae have different orientations of the inclusions, strongly suggesting that both the plagioclase and its albite twins existed prior to formation of the inclusions. Third, we have shown experimentally that the inclusions cannot have coexisted with their host plagioclase at 1100°C at 1 bar or at 5 kbar. Heating experiments on plagioclase with inclusions, intended to homogenize the inclusions and plagioclase, instead produced minute pockets of melt within the host plagioclase. Thus clearly the separate crystalline phases were not stable with respect to melting at that temperature, and melt formed in the experiments until all the oxide was used up. Fourth, magnetite and rutile, which are found touching each other in some inclusions, are not compatible at temperatures above ~400°C (Lindsley 1991, p. 85). We conclude that the inclusions could only have formed in the plagioclase

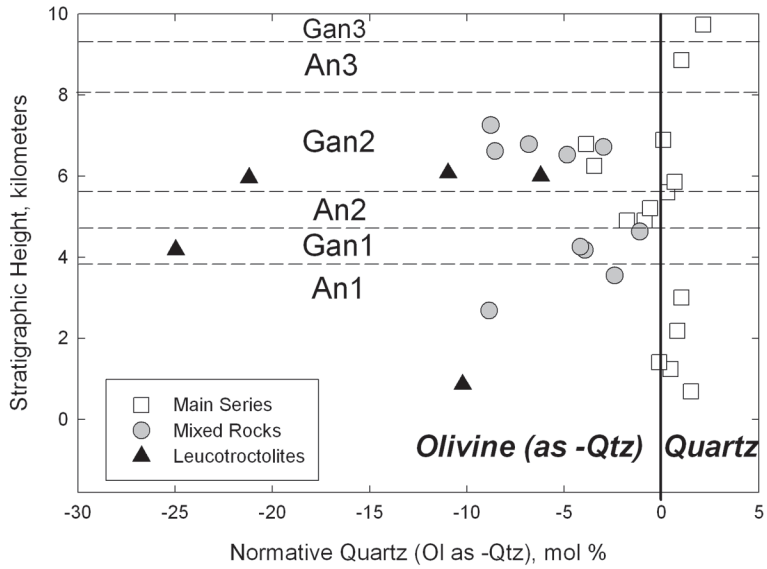

Fig. 12. Normative olivine or quartz (mol.%) for main-series rocks (open circles), mixed rocks (grey-filled circles), and leucotroctolites (black circles) in the Chugwater Anorthosite. Positive and negative numbers give percentages of normative quartz or olivine, respectively. Normative calculations assume that 15% of total iron is ferric; if this value varied by ±5%, the position of the zero point (no normative quartz or olivine) would vary by approximately ±1%. Main-series rocks have no modal and little or no normative olivine, suggesting that the main Chugwater anorthositic magma was not olivine-normative, and that olivine was contributed by admixture of leucotroctolitic magma with the Chugwater Anorthosite.

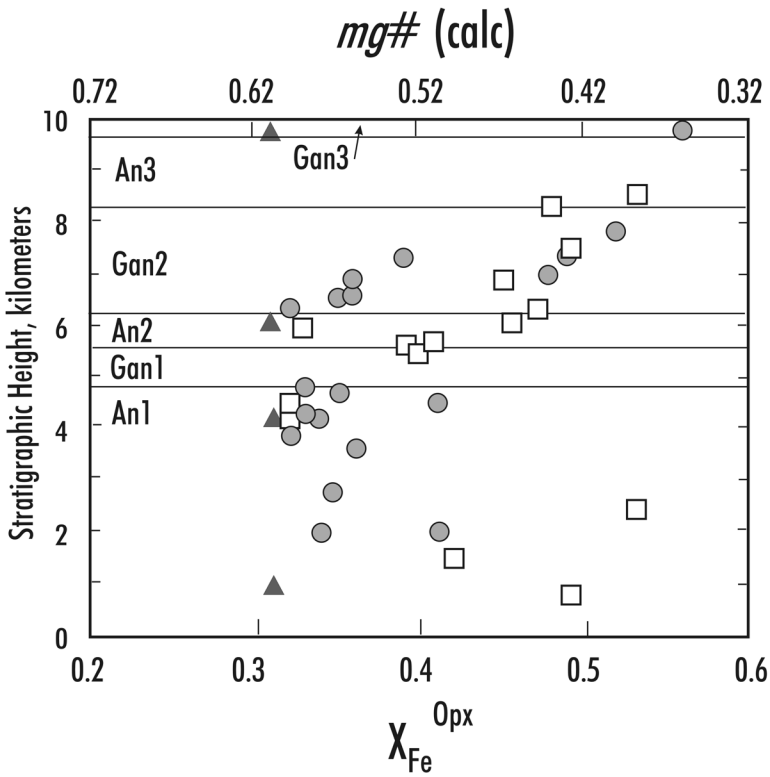

FIG. 13. X_{Fe}^{Opx} *versus* stratigraphic height in the Chugwater Anorthosite; symbols: main series: squares, mixed rocks: circles, and leucotroctolites: triangles. X_{Fe}^{Opx} is equal to Fe/(Fe + Mg) in orthopyroxene. It provides an estimate of whole-rock *mg#* through the empirical relationship $mg\# = 0.92 - X_{Fe}^{Opx}$. We do not know whether this relationship holds true for other anorthosites.

after the latter had cooled below 1100°C, and thus could not have been present at early stages of crystallization.

Origin (2), late-stage deposition by fluids, cannot be completely ruled out, but seems unlikely. Insofar as one can tell in thin section, the inclusions occupy volumes within the plagioclase; there is absolutely no evidence that they are associated with healed cracks or other planar features. Furthermore, the absence of inclusions from the rims of megacrysts (even where the core and rim compositions of plagioclase are virtually identical) and from plagioclase of nearby leucotroctolite argues against deposition from a pervasive fluid. By elimination, we conclude that case (3), origin of the oriented inclusions by exsolution, is the best explanation. Such an origin, also suggested by Anderson (1966), is most compatible with the preferred orientation and the extreme thinness of the platy inclusions. It is also the only plausible explanation for the distribution of inclusions in the spectacularly zoned iridescent plagioclase crystals in sample BM289 (5935 m level). Plagioclase compositions range from An_{52} to An_{57}, corresponding to interference colors from blue to red. Oxide inclusions occur *only in the blue resorbed cores* (which are interpreted to represent the plagioclase composition prior to mixing with high-An troctolite); they are absent from all the many zoned overgrowth layers, which are interpreted to have formed following repeated injections of the troctolite at the level of final emplacement. Oxide lamellae are absent even from zones having the same An content as the cores, so this cannot be a simple bulk-composition effect. Thus it seems clear that the Fe–Ti oxide lamellae in the Chugwater Anorthosite do not form in plagioclase that crystallized *at the depth of emplacement in the middle crust*. And as the plagioclase in BM289 cooled slowly enough to permit feldspar exsolution (hence the iridescence), the absence of Fe–Ti oxide lamellae is unlikely to be a kinetic effect. We conclude that feldspar that crystallized at greater pressure (hence also higher temperature in H_2O-poor melts) may have incorporated greater amounts of TiO_2

(~0.3–0.4 wt%), thereby permitting ilmenite and rutile lamellae to form, whereas plagioclase forming at shallower depths simply did not dissolve that much TiO_2.

That interpretation is supported by the experiments reported by Scoates & Lindsley (2000). They melted a composition containing 2.9 wt% TiO_2 and 16.7 wt% $FeO^{(T)}$ at 10 kbar and 1235°C and crystallized it at the same temperature (1130°C) but at two different pressures: 10 kbar and 5 kbar (the latter pressure to simulate decompression of an upwelling magma). Both experiments produced nearly identical plagioclase in terms of major elements (~An_{53}), but the plagioclase formed at 10 kbar contained 0.32–0.37 wt% TiO_2, approximately twice as much as that formed at 5 kbar (0.13–0.20 wt%). In contrast, iron contents of plagioclase were essentially independent of pressure: 0.69–1.04 wt% FeO at 10 kbar, 0.67–1.13 wt% at 5 kbar. The TiO_2 contents of the plagioclase crystallized at 10 kbar are close to the

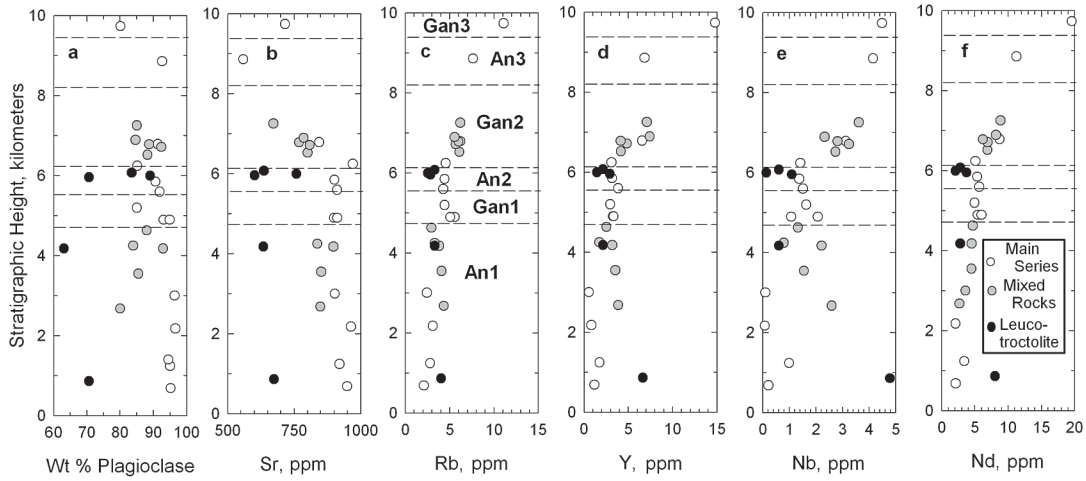

FIG. 14. Variation with stratigraphic height of (a) plagioclase content, (b) Sr, (c) Rb, (d) Y, (e) Nb, and (f) Nd in the Chugwater Anorthosite.

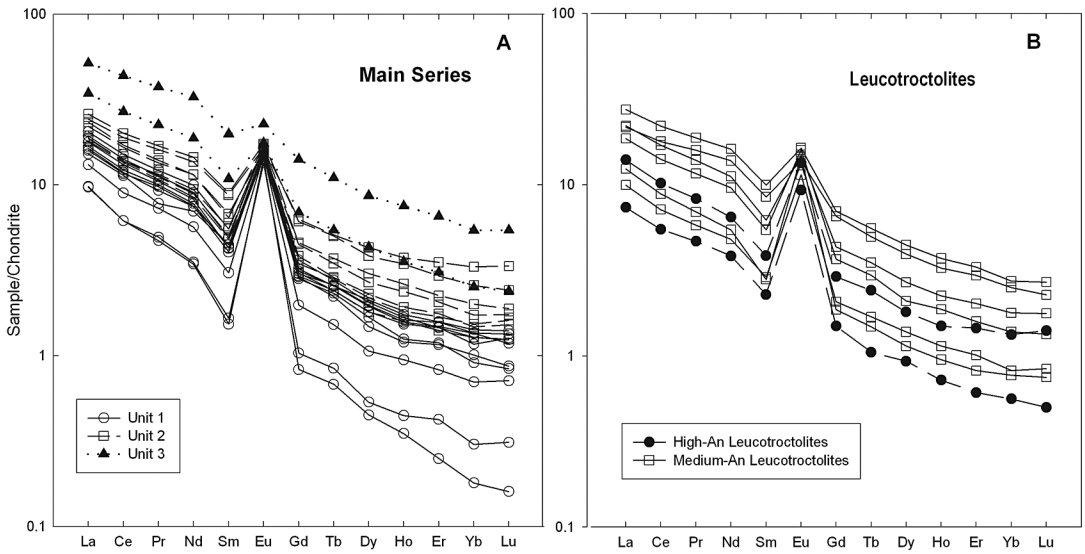

FIG. 15. Rare-earth elements (chondrite-normalized; Boynton 1984) in the main series and mixed rocks of the Chugwater Anorthosite. a. Main series: Unit 1 (An1 + Gan1), Unit 2 (An2 + Gan2), and Unit 3 (An3 + Gan3); b. leucotroctolites.

bulk compositions of ilmenite-bearing plagioclase in the Chugwater Anorthosite.

If one accepts the exsolution origin of the Fe–Ti oxide lamellae, then several interesting implications emerge. The restriction of the inclusions to plagioclase cores strongly suggests that the conditions at which the cores formed favored sufficient solubility of Fe- and especially of Ti-bearing components to allow the later exsolution. Most likely, these conditions were those at which megacrysts and other plagioclase entrained in the Chugwater Anorthosite originally crystallized, presumably a deep magma chamber. If this is so, then the presence of the ilmenite lamellae provides a simple petrographic means to distinguish "intratelluric" plagioclase from that which crystallized *in situ*, either directly from melt or during neoblastic recrystallization.

Black plagioclase is fairly common in a variety of igneous rocks, but we suggest that in many such cases, the plagioclase gets its color from inclusions of Ti-*poor* magnetite. We further suggest that it is the Ti-*rich* inclusions that may be diagnostic of plagioclase that formed at considerable depths. If that criterion is valid, then we conclude that very approximately one-half of the plagioclase now present in the main-series Chugwater Anorthosite was brought in to the level of emplacement as entrained crystals; the remaining half must then either have crystallized from the melt that accompanied the crystals into the level of emplacement, or have lost the oxide inclusions during deformation and neoblastic recrystallization.

Origin and nature of the parent melt

There are three main ways in which rocks with high contents of plagioclase, *i.e.,* anorthosites, could potentially form: (1) crystallization from a hyperfeldspathic magma, (2) formation from a melt having a high proportion of entrained plagioclase crystals, and (3) removal of most of the residual melt after much plagioclase but relatively small amounts of ferromagnesian minerals had crystallized. We believe that all three mechanisms may have been important in the formation of the Chugwater Anorthosite.

The origin of feldspar-rich melts through a two-stage process is a well-recognized model for anorthosite genesis (Morse 1968, Emslie 1985, Longhi & Ashwal 1985, Longhi *et al*. 1993). The first stage is crystallization of a mantle-derived melt at the base of the crust. The high-pressure conditions at the base of the crust have two major effects on the crystallization of basaltic melt. First, the crystallization fields for olivine and especially pyroxenes expand with increasing pressure at the expense of plagioclase (Fram & Longhi 1992, Scoates & Lindsley 2000), allowing the proportions of plagioclase components to build up in the liquid, and second, the initial plagioclase to crystallize is relatively sodic (Longhi *et al*. 1993, Scoates & Lindsley 2000). In this "standard model" of anorthosite genesis, the dense olivine and pyroxene settle to the bottom of the low-level magma chamber, effectively removing them prior to emplacement into the crust. The second advantage is that, owing to its compressibility at these pressures (see Fig. 12 of Scoates 2000), the residual basaltic melt is much denser than plagioclase. Thus when plagioclase eventually crystallizes, it floats to the top of the chamber. Finally, this plagioclase-rich mush at the top of the chamber becomes gravitationally unstable and rises diapirically into the crust, ultimately forming anorthosite as much of the residual liquid is expelled through a vague process called "filter-pressing". However, this model alone cannot fully explain layered bodies like the Poe Mountain Anorthosite and the Chugwater Anorthosite, which appear to have crystallized and differentiated in mid-crustal-level magma chambers.

Wiebe (1990, 1992) has proposed a variation on this "standard model" to explain the production of hyperfeldspathic melts, magmas containing greater proportions of plagioclase components than could be produced by cotectic crystallization alone. In his model, the plagioclase-rich portion of the deep magma chamber is reheated, probably through emplacement of fresh mantle-derived melt that provides heat but relatively little mass. A portion of the floating plagioclase crystals is resorbed, and since much of the ferromagnesian minerals that had crystallized along with the plagioclase had settled to the bottom of the chamber and would be unavailable for resorption, the resulting melt would be hyperfeldspathic. A further outcome of this mechanism is that the resulting melt could have a positive europium anomaly, a characteristic of many high-Al gabbros that have been proposed as possible parents for anorthosites (*e.g.,* Mitchell *et al*. 1995, Scoates & Mitchell 2000). Note that adiabatic decompression of the mush upon ascent into the crust could also result in minor resorption of plagioclase; Longhi *et al*. (1999) calculated that a pressure release from 13 to 4 kbar could remelt as much as 4% of the suspended plagioclase.

In an earlier section, we suggested on the basis of Ti-rich inclusions that approximately one-half of the plagioclase now present in the Chugwater Anorthosite came in as entrained crystals that had formed at a considerably greater depth than the level at which the intrusion was emplaced. With this fraction in mind, we can make some educated guesses about both the fraction of crystals in the magma that produced the Chugwater Anorthosite, as well as its normative plagioclase content. The *total* feldspar in an anorthosite must reflect the contributions from entrained plagioclase crystals plus normative plagioclase in the melt, minus the feldspar content of interstitial liquid that was removed. However, the final proportions of entrained plagioclase depend only on the first and last of these. Figure 16 shows the *total* feldspar that could be produced by melts having 60, 65, and 70% normative feldspar and carrying varying amounts of entrained plagioclase crystals. Consider a magma having 67% *normative*

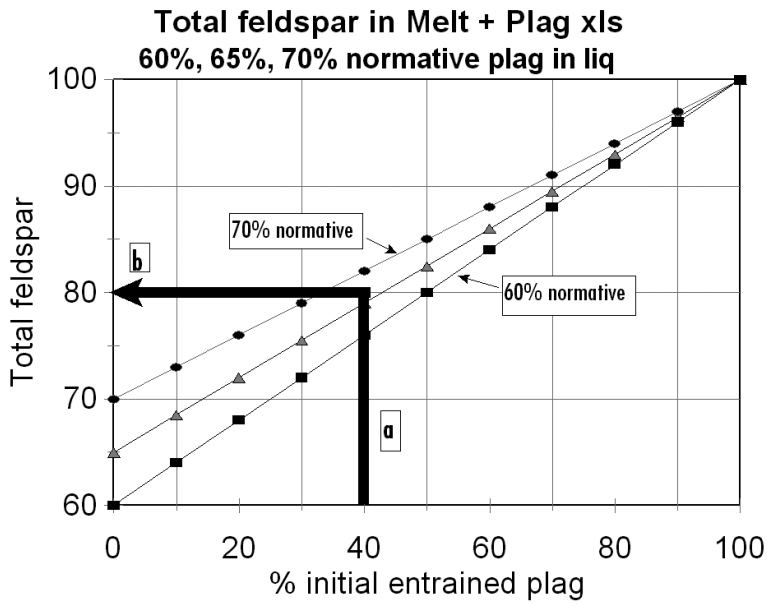

FIG. 16. Nomogram showing the total feldspar content that would be contributed (prior to removal of residual liquid) by magmas containing 60, 65, and 70% normative feldspar, plus varying amounts of entrained plagioclase crystals. The relationships hold for both weight and volume percent (if possible differences in thermal expansion are ignored). To use the diagram, one chooses an amount of entrained plagioclase (for example, 40% as in a), moves vertically to intersect the desired percentage of normative feldspar in the melt, and moves horizontally (b) to determine the total feldspar content (80% in the example chosen). Note that because the normative Or contents of Chugwater Anorthosite rocks and measured Or contents of their plagioclase are nearly identical, it is appropriate to treat all normative feldspar as "plagioclase".

feldspar and containing 40% *entrained* plagioclase (a in Fig. 16); its total feldspar content is 80% (b in Fig. 16) prior to filter pressing. Such a magma could crystallize directly to a gabbroic anorthosite without any removal of liquid. Assume that the interstitial liquid has the composition of ferrodiorite (Mitchell *et al*. 1996), which contains approximately 46% normative feldspar. Since the present average feldspar content of the solidified Chugwater Anorthosite is close to 90%, this would require removal of approximately 15–18% interstitial liquid, which would yield an anorthosite containing 50% entrained plagioclase and 40% plagioclase that crystallized *in situ*. Whereas small variations in the proportions of entrained plagioclase and normative feldspar content of the original melt could yield a similar result, other considerations suggest that the answer cannot vary greatly from this estimate.

Smaller proportions of entrained plagioclase would require either correspondingly greater normative feldspar contents of the magma (thus an increasingly greater hyperfeldspathic character) or removal of correspondingly greater amounts of interstitial liquid. Neither is attractive. Strongly hyperfeldspathic magma would require a greater contribution from the Wiebe mechanism described above. Since that model requires an extra step (reheating), Ockham's razor suggests that it should be invoked as minimally as possible. And removing more interstitial liquid raises serious problems about where that liquid has gone, since only minor amounts of ferrodiorite are exposed in the vicinity of the Chugwater Anorthosite.

Higher proportions of entrained plagioclase are also problematical, as the viscosity of the magma increases exponentially with the crystal content (Marsh 1996). This leads to a conundrum: to make anorthosite, one wants a maximum fraction of entrained plagioclase (this is part of the attraction of the Morse – Emslie – Longhi – Ashwal model of anorthosite petrogenesis; the anorthosite is emplaced as a crystal-rich mush), but for movement and production of layers within a magma chamber, as interpreted for the Chugwater and Poe Mountain anorthosites, that fraction should be as small as possible so as to keep the viscosity relatively low! Marsh (1996) pointed out that there is a profound

change in the behavior of melts at ~55% crystallinity; at and above that proportion, they behave mainly like weak solids. The parents to Poe Mountain Anorthosite and Chugwater Anorthosite must have had a considerably smaller percentage of entrained plagioclase than 55%. As a compromise, we adopt the estimate that the average magma emplaced to form the Chugwater Anorthosite contained ~40% entrained plagioclase in a melt having ~67% normative feldspar. This assumed composition of melt is only mildly hyperfeldspathic, approximately 4–8% above the cotectic value. Approximately 4% hyperfeldspathic character could have resulted simply from adiabatic resorption of plagioclase, as the cotectic would shift away from plagioclase upon decompression during ascent into the crust (Lindsley & Emslie 1968, Fram & Longhi 1992, Longhi *et al*. 1999, Scoates 2000). Thus the contribution required from the Wiebe reheating mechanism need not be great.

Small volumes of fine-grained high-Al gabbros occur as dikes throughout the Laramie Anorthosite Complex and have been proposed as examples of melts that could have produced anorthosite plus residual ferrodiorite through polybaric fractionation (Mitchell *et al*. 1995). Although most of the high-Al gabbros are strongly olivine-normative, there are a few high-Al gabbros in group 1 of Scoates & Mitchell (2000) that are silica-saturated or nearly so and that have compositions similar to the magma that may have been the source for the main series of the Chugwater Anorthosite. An experimental study of stepwise fractional crystallization of a high-Al gabbro from the LAC strongly supports this hypothesis (Scoates & Lindsley 2000).

Relatively high silica activity and $f(O_2)$ of the Chugwater Anorthosite

Two puzzling aspects of the Chugwater Anorthosite are its relatively high silica activity (0.7 – 1.0 based on a quartz standard state; Fig. 10A) and relatively high $f(O_2)$; neither is a feature we might expect in a rock derived directly from the mantle. One possibility is that the parent was derived by remelting of Proterozoic crust, as advocated by Longhi *et al*. (1999). Frost *et al*. (2003, 2010) have pointed out that the Chugwater Anorthosite has the most mantle-like initial Nd and Sr isotopic ratios of the Laramie anorthosites (see also Fig. 15 of Scoates & Chamberlain 2003), but these ratios could also reflect remelting of Proterozoic crust that was only slightly older than the anorthosite itself. While the isotopic data alone cannot rule out a crustal origin, we prefer the simpler interpretation of a direct-mantle source. An explanation for both features could be the addition of SiO_2 to the Chugwater Anorthosite from the country rock during its ascent and fractionation. This additional silica would react out any olivine present, and through the QUILF reactions (Lindsley & Frost 1992), could also raise the $f(O_2)$. Unfortunately, the Chugwater Anorthosite occurs mainly south of the Cheyenne belt, where the dominant country-rock is Proterozoic material ~300 Myr older than the Chugwater Anorthosite; even substantial amounts of contamination might not show up in the Nd and Sr isotopic ratios (Scoates & Chamberlain 2003, Frost *et al*. 2010). Indirect evidence favoring crustal contamination of mantle-derived material is the fact that the highest values calculated for silica activity in parts of the main series are near 0.75, not greatly above those for olivine-saturation (0.67–0.70; Fig. 11).

Emplacement of the Chugwater Anorthosite and magmatic processes: crystallization in situ

There are several textural and geochemical features suggesting that the Chugwater anorthosite accumulated essentially in place. First, the pluton contains layering on all scales from kilometer to decimeter and displays fabrics and textures that are dominated by tabular plagioclase, a typically igneous morphology. Second, we see enrichments in incompatible elements with increasing stratigraphic level that are locally interrupted by excursions toward lower values. These excursions are most readily interpreted as recording replenishment of new magma within a magma chamber. These features would have been destroyed had the pluton been emplaced either in the solid state or as a mush with a high proportion of crystals.

We propose that the Chugwater Anorthosite crystallized within a magma chamber at a depth of approximately 10–12 km, as based on the available geobarometry. The magma chamber was filled by a series of injections of a mildly hyperfeldspathic magma with approximately 40% entrained plagioclase crystals, as outlined above. There were at least three major episodes of injection, corresponding to stratigraphic units 1, 2, and 3, but there may well have been more. Excursions in X_{Fe}^{Opx} (Fig. 13; a proxy for $1 - mg\#$) and in the abundances of trace elements (Fig. 14) suggest that there may have been at least eight or more replenishments of magma. There is permissive evidence from values of X_{Fe}^{Opx} that the magma that fed Unit 2 may have been marginally more magnesian compared to the units above and below. Figure 17 is a set of schematic diagrams illustrating the emplacement of the Chugwater Anorthosite as interpreted here.

The U–Pb radiometric dates on samples from near the bottom (BM136, 1404 m level, 1435.4 ± 0.5 Ma; baddeleyite; Scoates & Chamberlain 1995) and top (KM13, 8860 m level, 1436.0 ± 0.5 Ma; zircon; Frost *et al*. 2010) of the Chugwater Anorthosite are indistinguishable within analytical uncertainty, suggesting that all 10,000+ m may have been emplaced (or at least cooled through the closure temperatures for Pb diffusion in zircon and baddeleyite, ~1000°C) within a million years. We have no reason to suspect that all 10,000+ m existed as an open magma chamber at any given time, but it certainly appears that the entire body

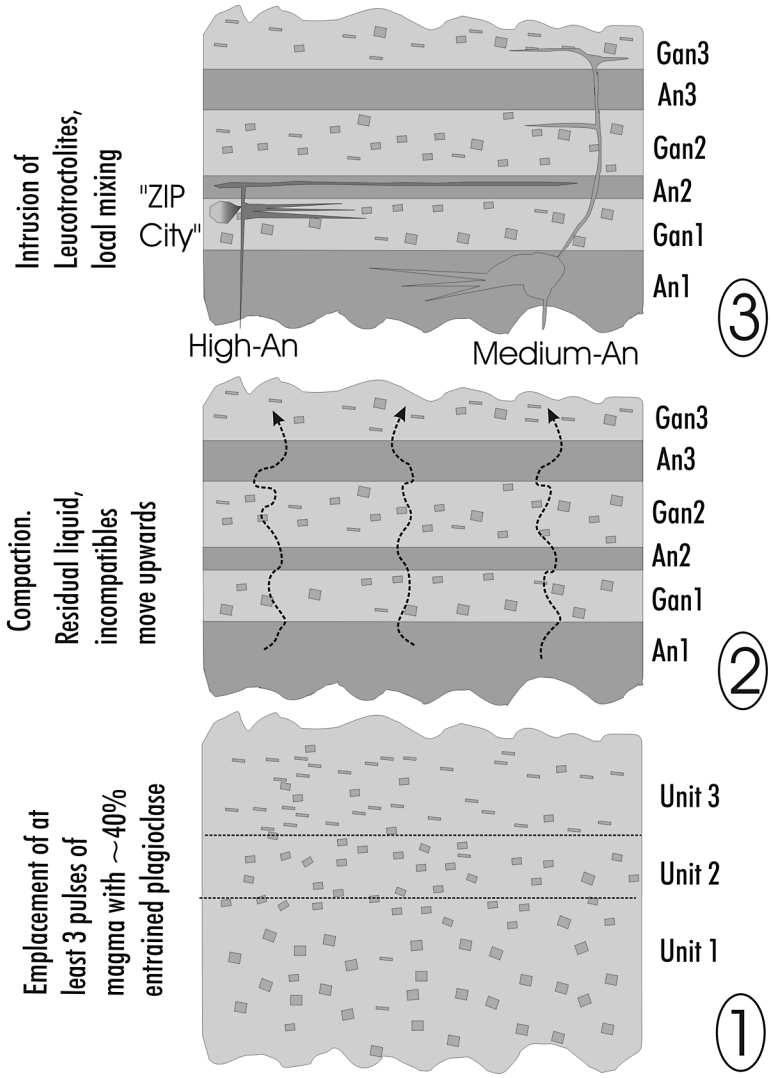

FIG. 17. Schematic diagrams showing stages in the development of the Chugwater Anorthosite. 1. Injection of at least three pulses of megacryst-rich magma, resulting in the three units of the main series. Silica activity in the magmas was 0.70–0.75, so little to no olivine formed from them. The injections need not have been simultaneous, but some residual liquid must have remained in older units as new pulses were emplaced. 2. Plagioclase accumulates near the bottom of each unit. Some residual liquid is removed (not shown), some migrates upward, producing an overall upward enrichment in incompatible elements. 3. At least two different leucotroctolitic magmas (one high-An, one medium-An) are injected into the Chugwater Anorthosite. Contacts with anorthosite layers are mainly sharp, suggesting that those layers behaved as solids at that stage. However, there was extensive mixing between leucotroctolite and the residual melts in gabbroic anorthosite layers, producing olivine-bearing mixed rocks. **Not shown**: Doming, which may well have been occurring during and after stages 2 and 3. All true anorthosites in the Chugwater Anorthosite show evidence of high-temperature deformation, suggesting that they were mainly solid at the time of the doming. In contrast, most gabbroic anorthosites show some, but lesser, degrees of deformation, suggesting that sufficient residual melt remained to accommodate much of the deformation in those layers by flow. Some leucotroctolites, especially those intruding Unit 1, are deformed, but most are not, suggesting that they were emplaced, or at least crystallized, relatively late in the doming process. Doming probably was contemporaneous with "filter pressing" to remove much residual melt. Draining away of dense residual liquid would have increased the gravitational instability of the Chugwater Anorthosite and thus could have contributed to the formation of doming.

was emplaced during that short an interval. Each of the three main units likely crystallized and fractionated independently, but several lines of evidence show that the lower units had not fully crystallized before the overlying one was emplaced. The most compelling evidence is the overall upward increase in incompatible trace elements (Figs. 14–15), which is best explained by escape of at least some residual liquids from lower levels into the units above. In addition, the fact that throughout the Chugwater Anorthosite, the anorthosite layers are distinctly more deformed than the adjacent layers of gabbroic anorthosite strongly suggests that at the time of deformation (presumably during doming; see below), the more mafic layers in each of the three main units still retained sufficient melt to accommodate the strain without major deformation of the plagioclase. This interpretation is further supported by the observation that the intruding leucotroctolites crosscut and have sharp boundaries against anorthosite layers but clearly mixed with the slightly more mafic layers.

Origin of the layering

As stated above, we attribute the existence of the three stratigraphic units 1, 2, and 3 to three major injections of magma. In particular, units An2 and An3 can readily be traced throughout the outcrop area of the stratigraphic Chugwater Anorthosite and are distinctive in their thickness (km scale). Unit An1 is less distinctive, in part because it contains numerous regions of gabbroic anorthosite that may result from multiple smaller injections of magma. It is possible that decameter-scale layers also reflect episodes of magma recharge, at least in part. However, our data simply do not permit tests of this hypothesis. As was the case for the Poe Mountain Anorthosite (Scoates 1994, 2000, Scoates *et al*. 2010), plagioclase must have accumulated as a network of cumulus grains on the floor of the magma chamber to form the various scales of layering. Since the host melt was hyperfeldspathic, only plagioclase was initially stable, and each layer would gain further plagioclase through adcumulus growth, thereby producing the true anorthosite layers. Eventually the melt would become pyroxene-saturated as well, giving rise to layers of gabbroic anorthosite as pyroxenes coprecipitated with plagioclase (Fig. 17, step 2). The origin of decimeter-scale layering in the Chugwater Anorthosite remains enigmatic. Deep weathering and the lack of fresh outcrops make detailed observation difficult, but modally graded layering, ascribed to density currents in the Skaergaard Intrusion and Duke Island Complex by Irvine (1987), for example, appears to be lacking. One possibility may be flow differentiation during emplacement of the magma, which, as discussed earlier, probably contained ~40% entrained plagioclase crystals. Flow during penecontemporaneous domal uplift of the Chugwater Anorthosite (see a later section) may have accentuated layer development.

Mixing with leucotroctolites

The main-series Chugwater Anorthosite, which mainly lacks modal olivine, was injected repeatedly by at least two types of leucotroctolites (Fig. 17, step 3). Both types are distinctly more magnesian than the main-series Chugwater Anorthosite; one has normative and modal compositions of plagioclase that are closely similar to the Chugwater Anorthosite, whereas the other is clearly more calcic. The first type could mix in small proportions with the Chugwater Anorthosite, with the only obvious evidence being an increase in orthopyroxene as olivine reacted with silica; once the excess silica was exhausted, small amounts of modal olivine would then appear. We see this in almost every instance where leucotroctolite intruded and mixed with gabbroic anorthosite. Plagioclase is little affected, except that it develops a rim lacking the Fe–Ti-rich lamellae typical of megacrystic plagioclase. In contrast, where the more calcic leucotroctolites have mixed, the plagioclase of the anorthosite shows reverse or oscillatory zoning.

Perhaps five percent of the mass of the Chugwater Anorthosite consists of these intruding leucotroctolites; another 10 to 15% has been demonstrably affected by mixing with them, although the overall mass fraction of leucotroctolite within the mixed rocks is probably small. One sample (BM273, 4180 m level) is a true troctolite; with 25% normative olivine and 63% feldspar, it is close to the cotectic proportions. It is equigranular and fine grained (1–2 mm), and almost certainly represents a liquid. All the other leucotroctolites have 70% normative feldspar or more, and thus probably reflect some degree of plagioclase accumulation, although most lack obvious plagioclase phenocrysts. An exception is BM52 (6000 m level), which has 89% normative feldspar and is thus nearly an anorthosite. We ascribe the high feldspar content of this sample to flow differentiation, with plagioclase phenocrysts concentrated in a region of presumably restricted flow. The genetic relationship of the leucotroctolites to the main-series Chugwater Anorthosite, if any, is unclear, although it is possible that they reflect less-evolved samples of the magma that gave rise to the main-stage anorthosites.

Origin and timing of the doming

The stratigraphic Chugwater Anorthosite forms an anticline plunging to the south and southwest, and is most likely a relic of a domal structure. Far too little country rock is exposed to be certain, but in the absence of known regional deformation at the time of emplacement of the Chugwater Anorthosite, we assume that the doming was produced during late-stage processes associated with emplacement of the Chugwater Anorthosite itself. A likely explanation is that the relatively light, plagioclase-rich cumulates became gravitationally unstable and began to rise. Much of the doming evidently took place while there was still residual liquid

present in the gabbroic anorthosite layers, where most of the deformation associated with the doming could have been accommodated by flow of melt between crystals. Indeed, this process may have aided in the development of decimeter-scale layering. In the plagioclase-rich layers, however, the deformation was accomplished through recrystallization of plagioclase *via* fast grain-boundary migration (Lafrance *et al*. 1996). That process occurs only at near-magmatic temperatures, which is compatible with the notion that some melt remained in more gabbroic layers. Some leucotroctolites intruding the Chugwater Anorthosite also show deformation, suggesting that they had been injected prior to the end of the deformation. Motion associated with the doming may explain why we find no obvious roof to the Chugwater Anorthosite, for example a horizon of relatively fine-grained leucogabbro; in the one place where the exposures are good, gabbroic anorthosite of Unit 3 is in direct contact with partially melted pelitic rocks. We have no way of estimating how much vertical displacement was associated with the doming.

Significance of the "structural boundary"

As noted in an earlier section, the anorthositic rocks to the south and southeast of the "structural boundary" (Fig. 2) have distinctly different orientations and are more strongly deformed, even though they are indistinguishable petrographically and chemically from the "stratigraphic Chugwater Anorthosite". We conclude that these rocks were a part of the Chugwater Anorthosite that had a different deformational history. We can only speculate about what led to the different deformational histories, but one possibility is that the Chugwater Anorthosite east and south of the "structural boundary" simply underwent an earlier and possibly stronger doming event. Another is that it was strongly affected by the emplacement of the Maloin Ranch Pluton, a basinal structure plunging to the southeast (Kolker & Lindsley 1989). Permissive support for this notion is provided by the presence of inclusions of highly deformed, high-An anorthosite near the boundary between the Chugwater Anorthosite and the Maloin Ranch Pluton as well as along the structural boundary within the Chugwater Anorthosite. In the southeast, the structural boundary appears to involve truncation of the An1, Gan1, and An2 units by the broadly curving upper units (Gan2, An3, Gan3); however, the picture is obscured by later (Laramide?) faulting, Whatever the causes, these deformations appear to have been mainly late-magmatic, as the associated deformation of the plagioclase occurred at a high temperature. However, local concentrations of epidote near the "structural boundary" suggest that deformation there must have continued down to low temperatures.

Clearly, the high-An inclusions associated with the boundaries are older than the Chugwater Anorthosite, but we have no idea just how much older. They typically are so deformed that they appear like granulated sugar. Our effort to extract datable material from one was unsuccessful. One possibility is that they are coeval with the 1.76 Ga Horse Creek anorthosite, which also is high in An. Another is that they are barely older than the Chugwater Anorthosite, but that like the Chugwater Anorthosite rocks south and southeast of the "structural boundary", they underwent strong deformation just prior to incorporation along the boundary.

Extraction of residual liquid; nature of "filter-pressing"

We estimated above that to achieve its present bulk composition, the Chugwater Anorthosite must have lost approximately 15–18% of its mass, the residual liquid, which is presumed to have a composition close to that of some of the ferrodiorites found in the Laramie Anorthosite Complex. This raises two important questions: (1) where is that mass now, and (2) by what mechanism was it removed? Some residual melt from the lower portions of the Chugwater Anorthosite moved upward, as evidenced by the up-section increase in incompatible elements. Although ferrodiorites are abundant both as dikes and pods in the Chugwater Anorthosite and adjacent rocks, their exposed mass is trivial compared to the amount needed to achieve mass balance. Thus much residual melt must have been removed from the present outcrop area of the Chugwater Anorthosite, leaving only small, volumetrically insignificant pockets and intrusions of ferrodiorite as evidence of this much larger volume. One very real possibility is that the dense residual liquids drained down-dip during the doming; indeed, the removal of dense material would increase the gravitational instability believed to have caused the doming and would accelerate it. Thus much of the residual liquid may lie below the present levels of exposure. In addition, a concept called "filter-pressing" is commonly invoked to explain the expulsion of trapped liquid, but to our knowledge no one has yet proposed a viable mechanism to accomplish it. One possibility would be the nucleation and expansion of a late vapor phase that might drive the trapped liquids to regions of lower pressure. Such a mechanism has been invoked for the formation of diktytaxitic texture in basalts (Fuller 1931, 1938). In diktytaxitic basalts, the gas-filled angular interstices remain, producing the distinctive "net-like" texture of these rocks. In an anorthosite at 3–4 kbar pressure, however, the cavities would collapse as the gas escaped, thereby contributing to the deformation so typical of anorthosites. If this mechanism had been operative in the Chugwater Anorthosite, quite clearly, given the high temperatures and relatively anhydrous assemblage inferred for it, the vapor could not have been water-rich. Although space precludes a detailed discussion here, there is substantial direct (Frost &

Touret 1989) and indirect evidence to suggest that the vapor may have been C–O rich, perhaps a mixture of CO and CO_2.

Conclusions

The Chugwater Anorthosite has a mappable magmatic stratigraphy totaling at least 8,000 meters, and probably more than 10,000 meters. Its main series comprises three major units, each with a dominantly anorthosite (>90 vol.% plagioclase) base and gabbroic anorthosite (80–90 vol.% plagioclase) upper portion. Most of the plagioclase in the main series is $An_{50–55}$; olivine is essentially absent. Layering, mostly modal but in places textural as well, occurs on scales from decimeters to decameters. The main series was produced by three major injections of mildly hyperfeldspathic magma containing approximately 40 vol.% entrained plagioclase megacrysts. The main series was repeatedly intruded by at least two leucotroctolitic magmas. Contacts of leucotroctolite are sharp against anorthosite but diffuse against gabbroic anorthosite; petrographic evidence shows mixing between leucotroctolite and the residual liquid of gabbroic anorthosite, indicating that the latter had not completely solidified at the time of intrusion. Prior to final solidification, the Chugwater Anorthosite was domed, probably as a result of gravitational instability of plagioclase-rich material. Removal of dense residual liquid (ferrodiorite) by filter pressing probably contributed to that instability.

Although massif anorthosites are generally considered to have been emplaced as crystal-laden diapirs (Ashwal 1993), the Chugwater anorthosite, like its sister the Poe Mountain anorthosite, is best considered as a plagioclase-rich layered intrusion. The direct evidence for crystallization from an open magma chamber is more subtle in the Chugwater anorthosite than in the Poe Mountain anorthosite, which records features such as scour marks and magmatic "drop stones" (Scoates 1994, 2000, 2002, Scoates *et al.* 2010). Nonetheless, the evidence is strong enough to support the contention that the Chugwater anorthosite formed by processes that are not very different from those found in other mafic–ultramafic layered igneous intrusions, except for the fact that the major cumulus mineral was plagioclase, rather than olivine or pyroxene.

Acknowledgements

We thank Jon Philipp, Goeff Rawling, and Patti Bleifus for assistance during the field work, William Meurer, Jeremy Mitchell, and Allan Kolker for chemical analyses, and Gregory Symmes, Susan Swapp, and Bob Rapp for electron-probe analyses. DHL thanks the Université Libre de Bruxelles for a productive sabbatical in 1997–98, under the auspices of a University International Chair, during which much of this report was prepared. This work was supported by NSF grants EAR–9218329 and its predecessors to DHL, and EAR–9017465 and EAR–9218360 to BRF and CDF. Constructive reviews by John Longhi, Tony Morse, and Mike Hamilton improved the manuscript; we heartily thank them. It is a pleasure to dedicate this paper to the memory of Ron Emslie. Ron infected us all with his enthusiasm for anorthosites, some in the field, some in the lab, all through discussions and his contributions to the literature. We miss him.

References

Allmendinger, K. D., Brewer, J. A., Brown, L. D., Kaufman, S., Oliver, J. E. & Houston, R.S. (1982): COCORP profiling across the Rocky Mountain front in Southern Wyoming. 2. Precambrian basement structure and its influence on Laramide deformation. *Geol. Soc. Am., Bull.* **93**, 1253-1263.

Andersen, D.J., Lindsley, D. H. & Davidson, P.M. (1993): QUILF: a PASCAL program to assess equilibria among Fe–Mg–Mn–Ti oxides, pyroxenes, olivine, and quartz. *Comput. Geosci.* **19**, 1333-1350.

Anderson, A.T. (1966): Mineralogy of the Labrieville anorthosite, Quebec. *Am. Mineral.* **51**, 1671-1711.

Ashwal, L.D. (1993): *Anorthosites*. Springer-Verlag, Berlin, Germany.

Ball, S.H. (1907): Titaniferous iron ore of Iron Mountain, Wyoming: contribution to economic geology. *U.S. Geol. Surv., Bull.* **315**, 206-212.

Barnichon, J.D., Havenith, H., Hoffer, B., Charlier, R., Jongmans, D. & Duchesne, J.-C. (1999): The deformation of the Egersund–Ogna anorthosite massif, south Norway: finite-element modelling of diapirism. *Tectonophysics* **303**, 109-130.

Bowen, N.L. (1917): The problem of the anorthosites. *J. Geol*, **25**, 209-243.

Boynton, W.V. (1984): Geochemistry of the rare earth elements: meteorite studies. *In* Rare Earth Element Geochemistry (P. Henderson, ed.). Elsevier, Amsterdam, The Netherlands (63-114).

Brewer, J.A., Allmendinger, R.W., Brown, L.D., Oliver, J.E. & Kaufman, S. (1982): COCORP profiling across the Rocky Mountain Front in southern Wyoming. 1. Laramide structure. *Geol. Soc. Am., Bull.* **93**, 1242-1252.

Buddington, A.F. (1939): Adirondack igneous rocks and their metamorphism. *Geol. Soc. Am., Mem.* **7**.

Darton, N.H., Blackwelder, E. & Siebenthal, C.E. (1910): Laramie–Sherman Folio. *U.S. Geol. Surv., Geologic Atlas of the United States, Folio* **173**.

Davidson, P.M. & Lindsley, D.H. (1989): Thermodynamic analysis of pyroxene – olivine – quartz equilibria in the system CaO–MgO–FeO–SiO_2. *Am. Mineral.* **74**, 18-30.

DeVore, G.W. (1975): The role of partial melting of metasediments in the formation of the anorthosite – norite – syenite complex, Laramie Range, Wyoming. *J. Geol.* **83**, 749-762.

Eberle, M.M.C. (1983): *Genesis of the Magnetite–Ilmenite Deposit at Iron Mountain, Laramie Anorthosite Complex, Wyoming*. M.S. thesis, University of Colorado, Boulder, Colorado.

Emslie, R.F. (1970): The Geology of the Michikamau intrusion, Labrador. *Geol. Surv. Can., Pap.* **68-57**.

Emslie, R.F. (1985): Proterozoic anorthosite massifs. *In* The Deep Proterozoic Crust in the North Atlantic Provinces (A.C. Tobi & J.L.R. Touret, eds.). D. Reidel Publishing Company, Dordrecht, The Netherlands (39-60).

Emslie, R.F., Hamilton, M.A. & Thériault, R.J. (1994): Petrogenesis of a mid-Proterozoic anorthosite – mangerite – charnockite – granite (AMCG) complex: isotopic and chemical evidence from the Nain Plutonic Suite. *J. Geol.* **98**, 539-558.

Fountain, J.C., Hodge, D.S. & Hills, F.A. (1981): Geochemistry and petrogenesis of the Laramie Anorthosite Complex, Wyoming. *Lithos* **14**, 113-132.

Fowler, K.S. (1930a): The anorthosite area of the Laramie Mountains, Wyoming. 1. Geomorphologic history. *Am. J. Sci.* **219**, 305-315.

Fowler, K.S. (1930b): The anorthosite area of the Laramie Mountains, Wyoming. 2. Petrographic and structural discussion. *Am. J. Sci.* **219**, 373-403.

Fram, M.S. & Longhi, J. (1992): Phase equilibria of dikes associated with Proterozoic anorthosite complexes. *Am. Mineral.* **77**, 605-616.

Frey, E. (1946a): Exploration of the Shanton iron-ore property, Albany County, Wyoming. *U.S. Bureau of Mines, Rep. Invest.* **3918**.

Frey, E. (1946b): Exploration of Iron Mountain titaniferous magnetite deposits, Albany County, Wyoming. *U.S. Bureau of Mines, Rep. Invest.* **3968**.

Frost, B.R., Frost, C.D., Lindsley, D.H., Scoates, J.S. & Mitchell, J.N. (1993): The Laramie Anorthosite Complex and the Sherman Batholith: geology, evolution, and theories for origin. *In* Geology of Wyoming 1 (A.W. Snoke, J.R. Steidtmann & S.M. Roberts, eds.). *Geol. Surv. Wyoming, Mem.* **5**, 119-161.

Frost, B.R. & Lindsley, D.H. (1992): Equilibria among Fe–Ti oxides, pyroxenes, olivine, and quartz. II. Application. *Am. Mineral.* **77**, 1004-1020.

Frost, B.R., Lindsley, D.H. & Andersen, D.J. (1988): Fe–Ti oxide–silicate equilibria: assemblages with fayalitic olivine. *Am. Mineral.* **73**, 727-740.

Frost, B.R. & Touret, J.L.R. (1989): Magmatic CO_2 and saline melts from the Sybille monzosyenite, Laramie Anorthosite Complex, Wyoming. *Contrib. Mineral. Petrol.* **103**, 178-186.

Frost, C.D., Chamberlain, K.R., Frost, B.R. & Scoates, J.S. (2000): The 1.76-Ga Horse Creek anorthosite complex, Wyoming: a massif anorthosite emplaced late in the Medicine Bow orogeny. *Rocky Mountain Geol.* **35**, 71-90.

Frost, C.D., Frost, B.R., Lindsley, D.H. & Chamberlain, K.R. (2003): Role of limited crustal assimilation in the evolution of three distinct anorthosite types in the Laramie Anorthosite Complex, Wyoming. *Geol. Soc. Am., Abstr. Programs* **35**, 394.

Frost, C.D., Frost, B.R., Lindsley, D.H., Chamberlain, K.R., Swapp, S.M. & Scoates J.S. (2010): Geochemical and isotopic evolution of the anorthositic plutons of the Laramie Anorthosite Complex: explanations for variations in silica activity and oxygen fugacity in anorthosites. *Can. Mineral.* **48**, 925-946.

Fuhrman, M.L., Frost, B.R. & Lindsley, D.H. (1988): Crystallization conditions of the Sybille monzosyenite, Laramie Anorthosite Complex, Wyoming. *J. Petrol.* **29**, 699-729.

Fuller, R.E. (1931): The geomorphology and volcanic sequence of Steens Mountain in southeastern Oregon. *Univ. Washington, Publ. in Geology* **3**(1).

Fuller, R.E. (1938): Deuteric alteration controlled by the jointing of lavas. *Am. J. Sci.* **235**, 161-171.

Goldberg, S.A. (1984): Geochemical relationships between anorthosite and associated iron-rich rocks, Laramie Range, Wyoming. *Contrib. Mineral. Petrol.* **87**, 376-387.

Grant, J.A. & Frost, B.R. (1990): Contact metamorphism and partial melting of pelitic rocks in the aureole of the Laramie Anorthosite Complex, Morton Pass, Wyoming. *Am. J. Sci.* **290**, 425-472.

Hayden, F. (1871): *Preliminary Report of the United States Geological Survey of Wyoming and Portions of Contiguous Territories*. U.S. Government Printing Office, Washington, D.C.

Hild, J.H. (1953): Diamond drilling on the Shanton magnetite–ilmenite deposits, Albany County, Wyoming. *U.S. Bureau of Mines, Rep. Invest.* **5012**, 1-17.

Hodge, D.S., Owen, L.B. & Smithson, S.B. (1973): Gravity interpretation of the Laramie Anorthosite Complex, Wyoming. *Geol. Soc. Am., Bull.* **84**, 1451-1464.

Hodge, D.S., Smith, B.D. & Smithson, S.B. (1970): Quantitative geophysical study of petrogenesis of syenites related to Laramie anorthosite, Wyoming, U.S.A. *Lithos* **3**, 237-250.

Irvine, T.N. (1987): Layering and related structures in the Duke Island and Skaergaard intrusions: similarities, differences, and origins. *In* Origins of Igneous Layering (I. Parsons, ed.). D. Reidel Publishing Company, Dordrecht, The Netherlands (185-245).

KLUGMAN, M.A. (1966): Resume of the geology of the Laramie anorthosite mass. *The Mountain Geologist* **3**, 75-84.

KOLKER, A. & LINDSLEY, D.H. (1989): Geochemical evolution of the Maloin Ranch Pluton, Laramie Anorthosite Complex, Wyoming: petrology and mixing relations. *Am. Mineral.* **74**, 307-324.

LAFRANCE, B., JOHN, B.E. & SCOATES, J.S. (1996): Syn-emplacement recrystallization and deformation microstructures in the Poe Mountain anorthosite, Wyoming. *Contrib. Mineral. Petrol.* **122**, 431-440.

LINDSLEY, D.H. (1991): Experimental studies of oxide minerals. *In* Oxide Minerals: Petrologic and Magnetic Significance (D.H. Lindsley, ed.). *Rev. Mineral.* **25**, 69-106.

LINDSLEY, D.H. & EMSLIE, R.F. (1968): Effect of pressure on the boundary curve in the system diopside – albite – anorthite. *Carnegie Inst. Wash., Year Book* **66**, 479-480.

LINDSLEY, D.H. & FROST, B.R. (1992): Equilibria among Fe–Ti oxides, pyroxenes, olivine, and quartz. I. Theory. *Am. Mineral.* **77**, 987-1003.

LONGHI, J. & ASHWAL, L.D. (1985): Two-stage model for lunar and terrestrial anorthosites: petrogenesis without a magma ocean. Proc. 15th Lunar Planetary Science Conf. 2. *J. Geophys. Res.* **90**, suppl., C571-C584.

LONGHI, J., FRAM, M.S., VANDER AUWERA, J. & MONTIETH, J.N. (1993): Pressure effects, kinetics, and rheology of anorthositic and related magmas. *Am. Mineral.* **78**, 1016-1030.

LONGHI, J., VANDER AUWERA, J., FRAM, M.S. & DUCHESNE, J.-C. (1999). Some phase equilibrium constraints on the origin of Proterozoic (massif) anorthosites and related rocks. *J. Petrol.* **40**, 339-362.

MARSH, B.D. (1996) Solidification fronts and magmatic evolution. *Mineral. Mag.* **60**, 5-40.

MEURER, W.P., WILLMORE, C.C. & BOUDREAU, A. (1999): Metal redistribution during fluid exsolution and migration in the Middle Banded series of the Stillwater Complex, Montana. *Lithos* **47**, 143-156.

MITCHELL, J.N. (1993): *Petrology and Geochemistry of Dioritic and Gabbroic Rocks in the Laramie Anorthosite Complex, Wyoming: Implications for the Evaluation of Proterozoic Anorthosites*. Ph.D. dissertation, Univ. of Wyoming, Laramie, Wyoming.

MITCHELL, J.N., SCOATES, J.S. & FROST, C.D. (1995) High-Al gabbros in the Laramie Anorthosite Complex, Wyoming: implications for the composition of melts parental to Proterozoic anorthosite. *Contrib. Mineral. Petrol.* **119**, 166-180.

MITCHELL, J.N., SCOATES, J.S., FROST, C.D. & KOLKER, A. (1996): The geochemical evolution of anorthosite residual magmas in the Laramie Anorthosite Complex, Wyoming. *J. Petrol.* **37**, 637-660.

MORSE, S.A. (1968): Layered intrusions and anorthosite genesis. *In* Origin of Anorthosite and Related Rocks (Y.W. Isachsen, ed.). *New York State Museum and Science Service, Mem.* **18**, 175-187.

NEWHOUSE, W.H. & HAGNER, A.F. (1957): Geologic map of anorthosite areas, southeastern part of Laramie Range, Wyoming. *U.S. Geol. Surv., Mineralogical Investigations Field Studies Map* **MF119**.

SCOATES, J.S. (1994): *Magmatic Evolution of Anorthositic and Monzonitic Rocks in the Mid-Proterozoic Laramie Anorthosite Complex, Wyoming, USA*. Ph.D. dissertation, Univ. Wyoming, Laramie, Wyoming.

SCOATES, J.S. (2000): The plagioclase – magma density paradox re-examined and the crystallization of Proterozoic anorthosites. *J. Petrol.* **41**, 627-649.

SCOATES, J.S. (2002): The plagioclase – magma density paradox re-examined and the crystallization of Proterozoic anorthosites: a reply. *J. Petrol.* **43**, 1979-1983.

SCOATES, J.S. & CHAMBERLAIN, K.R. (1995): Baddeleyite (ZrO_2) and zircon ($ZrSiO_4$) from anorthositic rocks of the Laramie anorthosite complex, Wyoming: petrologic consequences and U–Pb ages. *Am. Mineral.* **80**, 1317-1327.

SCOATES, J.S. & CHAMBERLAIN, K.R. (1997): Orogenic to post-orogenic origin for the 1.76 Ga Horse Creek anorthosite complex, Wyoming, USA. *J. Geol.* **105**, 331-343.

SCOATES, J.S. & CHAMBERLAIN, K.R. (2003): Geochronologic, geochemical and isotopic constraints on the origin of monzonitic and related rocks in the Laramie anorthosite complex, Wyoming, USA. *Precamb. Res.* **124**, 269-304.

SCOATES, J.S. & FROST, C.D. (1996): A strontium and neodymium isotopic investigation of the Laramie anorthosites, Wyoming, USA: implications for magma chamber processes and the evolution of magma conduits in Proterozoic anorthosites. *Geochim. Cosmochim. Acta* **60**, 95-107.

SCOATES, J.S., FROST, C.D., MITCHELL, J.N., LINDSLEY, D.H. & FROST, B.R. (1996): Residual-liquid origin for a monzonitic intrusion in a mid-Proterozoic anorthosite complex: the Sybille intrusion, Laramie anorthosite complex, Wyoming. *Geol. Soc. Am., Bull.* **108**, 1357-1371.

SCOATES, J.S. & LINDSLEY, D.H. (2000): New insights from experiments on the origin of anorthosite. *Trans. Am. Geophys. Union* (*Eos*) **81**(48), V71B (abstr.).

SCOATES, J.S., LINDSLEY, D.H, & FROST, B.R. (2010): Magmatic and structural evolution of an anorthositic magma chamber: the Poe Mountain intrusion, Laramie anorthosite complex, Wyoming (USA). *Can. Mineral.* **48**, 851-885.

SCOATES, J.S. & MITCHELL, J.N. (2000): The evolution of troctolitic and high Al basaltic magmas in Proterozoic anorthosite plutonic suites and implications for the Voisey's Bay massive Ni–Cu sulfide deposit. *Econ. Geol.* **95**, 677-701.

SINGEWALD, J.T., JR. (1913): The titaniferous iron ores in the United States. *U.S. Bureau of Mines, Bull.* **64**, 111-1125.

SMITH, B.D., HODGE, D.S. & SMITHSON, S.B. (1970): Geology and geophysics of syenites associated with Laramie Anorthosite, Wyoming. *Rocky Mountain Geol.* **9**, 27-38.

STRECKEISEN, A.L. (1967): Classification and nomenclature of igneous rocks (final report of an inquiry). *Neues Jahrb. Mineral., Abh.* **107**, 144-214.

STRECKEISEN, A.L. (1976): To each plutonic rock its proper name. *Earth-Sci. Rev.* **12**, 1-33.

SUBBARAYUDU, G.V. (1975): *The Rb–Sr Isotopic Composition and the Origin of the Laramie Anorthosite–Mangerite Complex, Laramie Range, Wyoming*. Ph.D. dissertation, State University of New York at Buffalo, Buffalo, New York.

SUBBARAYUDU, G.V., HILLS, A.F. & ZARTMAN, R.E. (1975): Age and Sr isotopic evidence for the origin of the Laramie anorthosite–syenite complex, Laramie Range, Wyoming. *Geol. Soc. Am., Abstr. Programs* **7**, 1287.

WIEBE, R.A. (1990) Evidence for unusually feldspathic liquids in the Nain Complex, Labrador. *Am. Mineral.* **75**, 1-12.

WIEBE, R.A. (1992): Proterozoic anorthosite complexes. *In* Proterozoic Crustal Evolution (K.C. Condie, ed.). Elsevier, Amsterdam, The Netherlands (215-261).

XIROUCHAKIS, D. (1996): *Contact Metamorphism Adjacent to the Laramie Anorthosite Complex, Albany County, Wyoming*. M.S. thesis, University of Minnesota, Duluth, Minnesota.

Received December 15, 2008, revised manuscript accepted July 6, 2010.